GEORG-AUGUST-UNIVERSITÄT
GÖTTINGEN

Fakultät für
Physik

Bachelor's Thesis

Abschätzung des W + Jets Untergrundes aus Daten für W-Helizitätsstudien am ATLAS-Experiment

A data-driven estimate of the W + jets background for W-helicity studies at the ATLAS experiment

prepared by

Cora Fischer

from Eschwege

at the II. Institute of Physics

Thesis number:	II.Physik-UniGö-BSc-2011/02
Thesis period:	28th March 2011 until 4th July 2011
Supervisor:	Dipl. Phys. Andrea Knue Dr. Shabnaz Pashapour Dr. Kevin Kröninger
First referee:	Prof. Dr. Arnulf Quadt
Second referee:	Prof. Dr. Ariane Frey

Contents

1. Introduction

Particle physics is the science that tries to answer the question of what the fundamental components of matter are and how they interact. To answer these questions, particle accelerators are built in which particles are accelerated close to the speed of light and are brought to collisions. The particles produced as a result of these collisions are then detected in particle detectors. To explore physics processes on these small scales particles need to be collided at high energies, therefore particle physics is also denoted as high energy physics (HEP). With the commissioning of the Large Hadron Collider (LHC) at CERN, new energy scales are explored which enable high precision measurements and will hopefully answer open questions related to the Standard Model (SM) or theories like Supersymmetry. An introduction into the theoretical basics is given in Chapter 2.
One of the biggest challenges in elementary particle physics is the identification of particles in collision experiments. Therefore detectors are developed that measure the tracks and energies of particles. In addition to a high precision detector, efficient methods of event selection and background estimation are essential to gain a better understanding of the process under study.
In top quark studies, a good understanding of background processes is crucial to gain a precise determination of the top quark properties. Why is it interesting to study top quark properties? The top quark is the heaviest known elementary particle in the SM and with its mass of (173.3±1.1) GeV/c^2 as current world average [1] that is close to the scale of electroweak symmetry breaking. Due to its large mass, the top quark decays before it can hadronize. Therefore the top quark decay can be studied without any effects of hadronization. Thus the top quark is an interesting object for testing the SM or searching for processes that cannot be described within the SM. One of these studies is the measurement of the helicity of the W-boson in top quark decays. This measurement in particular requires a good understanding of background processes. This thesis presents studies towards the determination of the dominating W+jets background for W-helicity measurements. A template method is used to extract scale factors from data for Monte Carlo (MC) samples to get a better description of the W+jets background based on experimental results.

In Chapter 2, the Standard Model is briefly summarized followed by the introduction to top quark physics. An emphasis is placed on background processes regarding the semileptonic $t\bar{t}$ decay, in particular the production of W+jets and data-driven estimation methods of this background process. In Chapter 3, the experimental setup of the ATLAS detector is described. Chapter 5 continues with the event reconstruction containing object definitions and selection criteria. A description of the Monte Carlo simulation and the used MC samples for the analysis are given in Chapter 4. After the introduction of the relevant statistical tools in Chapter 6, the precise description of the background estimation procedure follows in Chapter 7. The results for the background estimation are presented in Chapter 8. Statistical uncertainties are evaluated. A summary of the studies and an outlook is given in Chapter 9.

2. Theoretical Basics

This chapter gives a theoretical overview on the Standard Model of Elementary Particle Physics in general and top quark physics in particular. As mentioned in Chapter 1, studies of the top quark properties provide an excellent environment for testing the Standard Model. So far no deviations of the SM predictions have been observed. Therefore the Standard Model can be seen as a successful model to describe the fundamental components of matter. Although no deviations have been found there are still some aspects not satisfactorily described by the SM. An introduction to the fundamental principles of the SM follows which gives a motivation towards studies of the top quark properties.

2.1. The Standard Model

The Standard Model describes the elementary particles and the interactions between them. Elementary particles are assumed to have no substructure. In the SM these elementary particles are divided into three families of leptons

$$\begin{pmatrix} \nu_e \\ e \end{pmatrix}, \begin{pmatrix} \nu_\mu \\ \mu \end{pmatrix}, \begin{pmatrix} \nu_\tau \\ \tau \end{pmatrix}$$

and three families of quarks

$$\begin{pmatrix} u \\ d \end{pmatrix}, \begin{pmatrix} c \\ s \end{pmatrix}, \begin{pmatrix} t \\ b \end{pmatrix}.$$

The leptons denoted as e, μ and τ are the electron, muon and tau-lepton with their associated neutrinos ν_e, ν_μ and ν_τ, respectively. The quark denotations u, d, c, s, t and b stand for *up*, *down*, *charm*, *strange*, *top* and *bottom*. The leptons and quarks collectively are known as the elementary fermions that all carry spin of s=1/2 [2]. Each fermion has an antiparticle partner with the same mass and spin but opposite electric charge (except for the electrically neutral neutrinos, where particle and antiparticle do not differ by the electric charge). The charges of the fermions are quoted in Table 2.2. The elementary

fermions interact via the exchange of the so-called *gauge bosons* that carry integer spin $s = 1$. The gauge bosons are the force carriers of the three fundamental forces strong, electromagnetic and weak that are described within the SM. Each of them couples to different types of charges. A summary of the three forces is given in Table 2.1. The

interaction	couples to	mediator	mass [GeV/c^2]	J^P
strong	colour	8 gluons (g)	0	1^-
electromagnetic	electric charge	photon (γ)	0	1^-
weak	weak charge	$W^{\pm}$, Z^0	$\approx 10^2$	1

Table 2.1.: The three interactions with their gauge bosons described in the SM. J denotes the total angular momentum and P the parity eigenvalue (only for those bosons that are eigenstates of the parity operator: $P(\vec{x}) = -\vec{x}$)

electromagnetic force is mediated by photons ($m_\gamma = 0$) which are electrically neutral. Since photons only couple to charge, they do not interact with the neutrinos. Furthermore, no self-coupling between photons is possible. The range of a force is typically proportional to the inverse of the mass of the mediator ($R \propto 1/m$) so the range of the electromagnetic force is compatible with infinity [1].

The weak force mediated by charged W-bosons and the neutral Z-boson acts on all fundamental fermions. These bosons only couple to left-handed[2] doublets of particles. Only the left-handed particles carry the so-called weak isospin T, which is quoted in Table 2.2 together with the third component T_3. The doublets consist of eigenstates of the weak interaction, called flavour-eigenstates, where the flavour-eigenstates of the $T_3 = -1/2$ quarks are mixings of the downtype quarks d, s and b described by the *CKM-Matrix* [2]. These mixings are denoted as d', s' and b' in Table 2.2. The weak gauge bosons do not couple to right-handed particles and therefore only right-handed singlets exist that are also quoted in Table 2.2. Only the charged currents from W-bosons are able to change the flavour of a particle. The range of the weak force is strongly limited due to the high masses of the corresponding gauge bosons.

Weinberg, Glashow and Salam combined the electromagnetic and weak forces to the *electroweak* force which is described by the $SU(2)_L \otimes U(1)_Y$ symmetry group. This group is generated by the weak isospin and the weak *hypercharge* (defined as $Y = 2Q - 2T_3$) [3–5]. $SU(2)_L$ is the unitary gauge group that describes the weak interaction where L denotes

[1] This refers to massless photons with infinite lifetime that can travel an infinite distance, while the magnitude of the force between two charges obeys the 'inverse square law'.

[2] The helicity is defined as the orthogonal projection of the spin of a particle on the direction of its momentum. Particles whose spin points opposite to the momentum are called *left-handed*, particles whose spin is parallel to the momentum are called *right-handed*. When the spin of a particle is orthogonal to its momentum then it is *longitudinally polarised*.

	fermion multiplets			T	T_3	Q [e]
leptons	$\begin{pmatrix} \nu_e \\ e^- \end{pmatrix}_L$	$\begin{pmatrix} \nu_\mu \\ \mu^- \end{pmatrix}_L$	$\begin{pmatrix} \nu_\tau \\ \tau^- \end{pmatrix}_L$	1/2	$+1/2$ $-1/2$	0 -1
	e^-_R	μ^-_R	τ^-_R	0	0	-1
quarks	$\begin{pmatrix} u \\ d' \end{pmatrix}_L$	$\begin{pmatrix} c \\ s' \end{pmatrix}_L$	$\begin{pmatrix} t \\ b' \end{pmatrix}_L$	1/2	$+1/2$ $-1/2$	$+2/3$ $-1/3$
	u_R	c_R	t_R	0	0	$+2/3$
	d_R	s_R	b_R	0	0	$-1/3$

Table 2.2.: Fermions and their corresponding weak isospin T with third component T_3 and charge Q [2].

the coupling to left-handed particles and $U(1)_Y$ is the unitary gauge group describing the electromagnetic interaction where Y indicates the hypercharge.
The strong force mediated by gluons only acts on particles that carry *colour charge* and is described by the $SU(3)_C$ group (C indicates the colour). The colour of particles is an additional quantum number that was introduced for quarks to describe experimental observations, e. g. the existence of the Ω-Baryon (sss) that would otherwise violate the Pauli principle. A quark can have one of the three colours red, green and blue (r,g,b)[3]. In nature one only observes colourless bound states like baryons (qqq) and mesons ($q\bar{q}$), thus no single quark can be observed (the q's do not necessarily represent the same quarks). This leads to the special character of the strong force described by *Quantum Chromo Dynamics* (QCD): The force between two quarks increases with increasing distance. If one wants to divide these quarks the energy in the field between these quarks increases to a point where a new $q\bar{q}$-pair will be produced. Instead of isolating them one produces another pair of quarks which makes it impossible to observe them as single particles. This phenomenon is known as *quark confinement*. The reason for this behaviour is the self-interaction between the gluons. This leads to "antiscreening"[4] of the colour charge. Thus the range of the strong force is that short although the gluons are massless.
The three forces together form the model through which the SM is denoted as

$$SU(3)_C \otimes SU(2)_L \otimes U(1)_Y.$$

The gauge theories that describe the interactions are based on the requirement of the Lagrangian $\mathscr{L}$ to be invariant under *local* phase transformations. These requirements lead to

[3] Antiquarks are carrying the anticolours $\bar{\mathrm{r}}, \bar{\mathrm{g}}, \bar{\mathrm{b}}$.
[4] The opposite effect of screening: the larger the distance to the colour charge the stronger it gets due to a cloud of gluons that is spread around it.

interaction terms in $\mathscr{L}$ which contain the gauge fields that describe the gauge bosons. The latter have to be massless in order to conserve $\mathscr{L}$ under local phase transformations. This contradicts the fact that the W and Z bosons are massive ($m_W = (80.399 \pm 0.023)$ GeV/c^2, $m_Z = (91.1876 \pm 0.0021)$ GeV/c^2 [2]). This problem is solved by introducing the so-called *Higgs-Mechanism* which is based on spontaneous symmetry-breaking that gives mass to each particle and predicts a further scalar ($s = 0$) particle, the *Higgs-boson*. The Higgs-particle is part of the SM but has not been observed so far.

Although the predictions of the SM have been consistent with experimental results up to now it cannot answer all questions concerning the fundamental composition of the universe. It does not include the gravity, it cannot predict parameters like the masses of the particles or mixing angles, thus more than 20 parameters remain arbitrary and have to be determined by experiments. Furthermore the issue of "dark matter" and "dark energy" that are assumed to make up $\sim 95\%$ of the mass density of the universe is not included in the SM [6]. The CP-violation in the quark sector described by the CKM-Matrix cannot alone explain the matter-antimatter asymmetry in the universe. Additionally, experiments have shown that the neutrino is not massless as assumed in the SM [2, 7].
All these questions demand further tests of the SM predictions. The top quark due to its properties is a good candidate for such tests and will be discussed in this thesis. Therefore an introduction to top quark physics is given in the following.

2.2. The Top Quark

With the discovery of the top quark in 1995 at the TEVATRON [8, 9] the third generation of quarks in the SM was completed . The top quark stands out from other SM elementary particles especially because of its large mass (see Chapter 1), resulting in a short life time of about $\tau \approx 5 \cdot 10^{-25}$ s [10]. The top quark decays before it hadronizes (hadronization time $\approx 10^{-23}$ s) and therefore no bound states containing top quarks (e. g. "toponium") exist [11, 12]. The branching ratio of the almost exclusive decay channel of $t \to W^+ + b$ exceeds 99.8% [13]. In this context the structure of the Wtb vertex is an interesting object to investigate in order to test SM predictions. In the SM this vertex has a $V-A$ structure (see Sect. 2.4). The analysis of the helicity of the W-boson (see section 2.4) gives the possibility to search for a possible $V + A$ contribution to this vertex.

2.2.1. Production

According to the SM, top quarks can be produced as single top or in pairs. The single top production can only be mediated by the weak interaction. Top quark pairs are produced via the strong interaction. In the following only the top quark pair production is described.

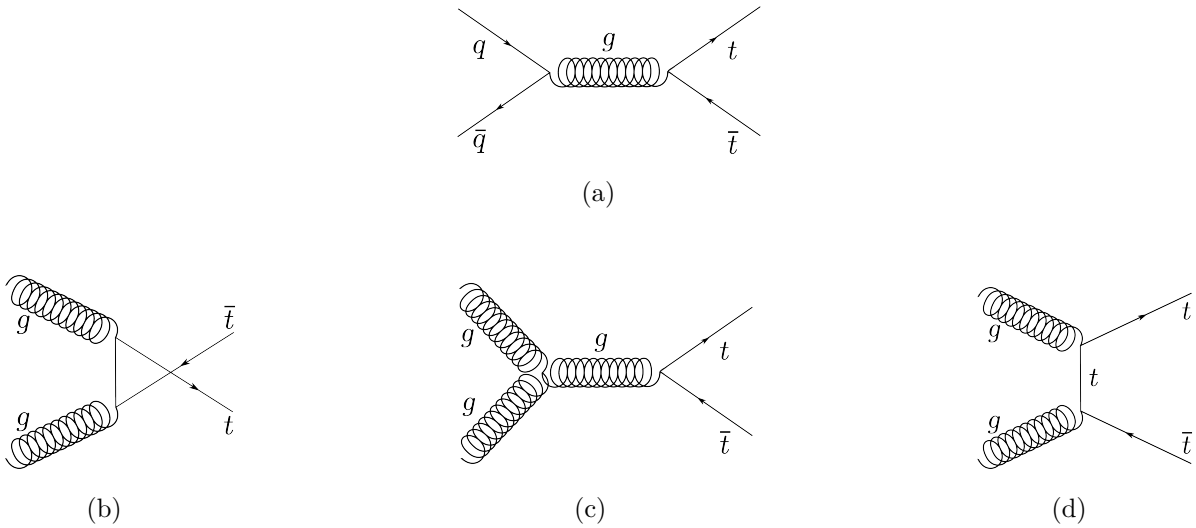

Figure 2.1.: LO $t\bar{t}$ production via $q\bar{q}$ annihilation (a) and via gg-fusion (b, c, d).

At leading order (LO), top quark pairs are produced via two different mechanisms: quark-antiquark annihilation and gluon-gluon fusion as depicted by Feynman-diagrams in Figure 2.1. Which process dominates depends on the types of hadrons that are used in collision experiments and their center-of-mass energy, $\sqrt{s}$. While the $q\bar{q}$ annihilation dominates at the TEVATRON (which is a $p\bar{p}$-collider), the gg-fusion is the dominant process at the LHC. Table 2.3 shows the fractions of $q\bar{q}$ annihilation and gg-fusion at both colliders with their center-of-mass energies [14, 15]. This dependency can be explained by the

Process	TEVATRON ($\sqrt{s}$=1.96 TeV)	LHC ($\sqrt{s}$=7 TeV)
$q\bar{q}$ annihilation	85%	20%
gg-fusion	15%	80%

Table 2.3.: Fractions of processes in which $t\bar{t}$-pairs are produced at TEVATRON and LHC.

parton density functions (PDF) inside the protons and antiprotons, respectively. Each parton carries a certain fraction of the proton momentum. The valence quarks inside the protons carry on average a higher fraction of the momentum than the sea quarks and gluons. For higher center-of-mass energies, a lower momentum fraction of the total proton

momentum is necessary to produce top quark pairs. In the low fraction region, gluons dominate over valence and sea quarks. Figure 2.2 shows a parameterization of PDFs for a proton with an energy of 85 GeV (PDFs created by the CTEQ working group) and illustrates the described behaviour, where x denotes the momentum fraction [16]. For antiprotons the curves are equally "shaped" but belong to the antiparticles, respectively (here $\bar{u}\bar{u}\bar{d}$ are the valence quarks that carry a higher momentum fraction on average).

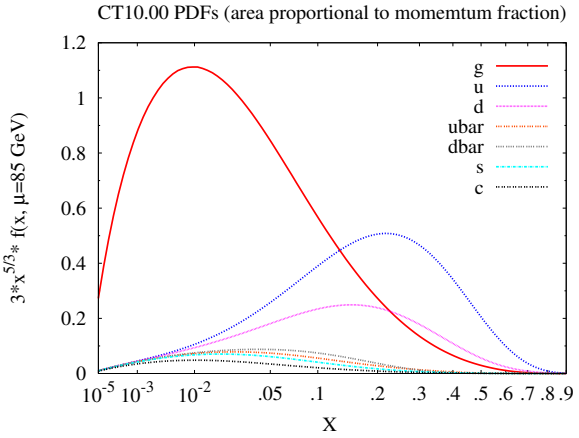

Figure 2.2.: CT10 parameterization of PDFs for a proton at $\mu = 85$ GeV by the CTEQ working group [16]. The y-axis is scaled in a way that the areas under the curves represent the total momentum fraction of partons belonging to the curve.

2.2.2. Decay

The top quark decays via the weak interaction almost exclusively into a W-boson and a b-quark. Due to the large top quark mass the W-boson can be produced as a real particle. The W-boson decays hadronically into quarks or leptonically into a charged lepton and its corresponding neutrino.

One distinguishes three different decay channels of top quark pairs with respect to the decay of the two W-bosons: the *fully-hadronic*, the *semileptonic* and the *dileptonic* channel. The fully-hadronic channel denotes the channel in which both W-bosons decay hadronically. It has the highest branching ratio of about 46.2 % [11], but the poorest signal-to-background ratio due to QCD multijet production. The semileptonic channel turns out to be the most appropriate channel for studies of $t\bar{t}$ events. The signature of the semileptonic channel consists of four jets, one charged lepton ℓ and a neutrino, which is recognized as missing transverse energy ($\not{E}_T$). Due to the large top quark mass, the jets have high transverse momenta in the final state. This signature makes it easier to distinguish the signal from background processes such as multijet production. The advantage

of the semileptonic channel compared to the dilepton channel is a higher branching ratio of 43.5 % compared to the one of the dilepton channel with 10.3 % [11]. In the dilepton channel both W-bosons decay leptonically. Therefore two neutrinos in the final state exist which can only be recognized by high $\not\!\!E_T$. This leads to an under-determined system of equations.
In the following, only final states containing one electron or one muon are studied for the reconstruction of the $t\bar{t}$ event. This includes leptonically decaying τ-leptons.

2.3. Background Processes

For a good understanding of processes under study, a good understanding of the relevant background processes is crucial. This is especially important in a W-helicity analysis: the challenge here is not only to separate the signal from the background but also to extract the three different helicity fractions in the signal. We concentrate on the signature of the semileptonic channel in $t\bar{t}$ events, which we investigate.
This signature can be produced as well by several background processes including single top, diboson [5], Z+jets and W+jets as well as multijet production. Some of these contain a leptonically decaying W-boson, such as WW, WZ, single top and W+jets events. In others like the multijet production the lepton is faked by a jet and the missing transverse energy $\not\!\!E_T$ is observed due to incomplete or inefficient reconstruction of jets or leptons. The latter one also applies to ZZ and Z+jets events. To distinguish these processes from the relevant $t\bar{t}$ process, one needs to apply several selection criteria. From all background events that contain a W-boson, the W+jets background is most likely to be selected. For low jet multiplicities the W+jets process has a high production cross section. Therefore it is the dominant background for semileptonic $t\bar{t}$ events which we want to investigate. The W+jets background differs from the searched signature by the requirement of at least four jets with high transverse momenta in the final state as well as eventually a b-tag for $t\bar{t}$ events (see Section 5.2). Thus processes beginning at $W + 4$ jets contribute to the background. To distinguish these events from the $t\bar{t}$-signal one needs to apply further selection cuts. In this sense it is always important to take care of the ratio of signal to background rejection because one can only make reasonable statistical statements if there are enough signal events left to study.
A closer look is taken at the production mechanism of a W-boson in association with jets in the following section.

[5] A diboson process is a process that consists of two of the weak gauge bosons, thus the contributions come from WW, WZ and ZZ processes.

2.3.1. *W*+Jets Production

The W-boson is produced via quark-antiquark collisions, $q\bar{q}' \rightarrow W$, where in our case the W decays leptonically. A concrete mechanism that dominates at the LHC and the TEVATRON is given by:

$$u + \bar{d} \rightarrow W^+ \text{ and } \bar{u} + d \rightarrow W^-$$

At the LHC the production ratio W^+/W^- exceeds unity because the LHC is a proton-proton collider. On average the momentum fraction of an *up* valence quark is higher than of a *down* valence quark in a proton, thus $u(x)/d(x) > 1$, where x is the momentum fraction (see Fig. 2.2). This production asymmetry of W^+ and W^- can be exploited in terms of the estimation of W+jets events in a $t\bar{t}$-selection sample (see 2.5).
The production of a W and additional jets involves gluons, e. g. $q\bar{q}' \rightarrow Wg$ and $gq \rightarrow Wq'$, that are radiated from quarks or other gluons. Figure 2.3 shows examples for the production of W+4 jets that contribute to the $t\bar{t}$ background.

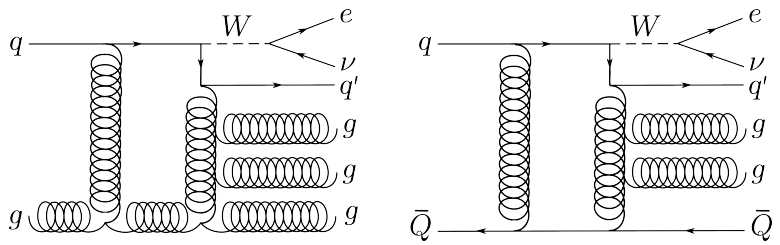

Figure 2.3.: Possible W+ 4 jets processes that contribute to the $t\bar{t}$ background in the semileptonic channel.

The production processes of higher jet multiplicities include higher numbers of vertices. Each vertex contributes to the amplitude of the process with an additional coupling α_s, the coupling 'constant' of the strong force (in fact the magnitude depends on the energy scale). Taking these additional contributions of α_s into account leads to the assumption that the ratio $(W + n \text{ jets})/(W + (n-1) \text{ jets})$ is approximately constant, thus independent of the number of jets. In this consideration some other effects are not regarded. For example the ratio $(W + 1 \text{ jet})/(W + 0 \text{ jets})$ has to be treated differently because of different production kinematics that also have to be taken into account. In the $W + 0$ process there are no reconstructed jets that recoil against the W-boson and therefore a different value for $(W + 1 \text{ jet})/(W + 0 \text{ jets})$ is predicted in contrast to the approximately constant $(W + n \text{ jets})/(W + (n-1)\text{jets})$ ratio [17, 18].
Understanding the circumstances of the W+jets production gives a basis for its background estimation (see Sect. 2.5).

2.4. Helicity of the *W*-Boson

In order to test the Wtb vertex structure one can analyse the helicity states of the W-boson. The top quark as a fermion has spin of $s = 1/2$ the same as the spin of the b-quark, whereas the W-boson is a particle with spin of $s = 1$. In the rest frame of the top quark, there are three possibilities for the spins as seen in Figure 2.4. The arrows indicate the direction of the spin, the thin ones the direction of flight of W and b.

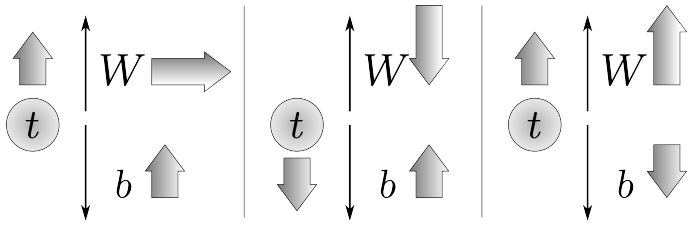

Figure 2.4.: Possible helicity states in the top quark decay: In the rest frame of the top quark the W-boson and the b-quark must have opposite momenta. Taking conservation of the angular momentum into account results in the three possibilities seen above: Left: longitudinally polarised, Middle: left-handed and Right: right-handed W-boson.

The vertex structure of the Wtb vertex plays an important role concerning the probability for each of the mentioned spin adjustments. The SM Lagrangian of the Wtb vertex is:

$$\mathscr{L} = -\frac{g}{\sqrt{2}}\bar{b}\gamma^{\mu}V_{tb}\frac{1}{2}\left(1-\gamma^{5}\right)tW_{\mu}^{-} + h.c.$$

V_{tb} is the CKM-Matrix element whose magnitude describes the branching ratio of the decay $t \to W^{+} + b$ which is almost equal to one (see Sect. 2.2). The $V - A$ vertex structure is visible in $\frac{1}{2}\gamma^{\mu}\left(1-\gamma^{5}\right)$ where $P_L = \frac{1}{2}\left(1-\gamma^{5}\right)$ denotes the left-handed projector which can be applied to the spinors t and $\bar{b}$ and shows the character of the electroweak force described in Sect. 2.1. The three relative fractions that represent the three different states illustrated in Fig. 2.4, are often denoted by F_{+} for a right-handed, F_{-} for a left-handed and F_0 for a longitudinally polarised W-boson. They are defined by the branching ratios:

$$F_{+} = \frac{\Gamma(t \to W_R + b)}{\Gamma}, \quad F_{-} = \frac{\Gamma(t \to W_L + b)}{\Gamma}, \text{ and } F_0 = \frac{\Gamma(t \to W_0 + b)}{\Gamma},$$

where Γ is the total decay width of the process $t \to W^+ + b$ and $\Gamma(t \to W_X + b)$ with the indices $X = R, L$ and 0 indicate the decay widths belonging to a W with the specific helicity states right-handed, left-handed and longitudinally polarised, respectively.
In comparison to the masses of the W-boson and the top quark, the mass of the bottom quark is relatively small. Massless particles carry negative helicity in weak interactions according to the SM and are therefore always left-handed in weak interactions. If one neglects the mass of the b-quark the consequence is that the possibility of a right-handed W^+ boson, which can be seen on the right side of Fig. 2.4, has to be excluded. If higher order terms in m_b are taken into account, thus not neglecting the b-quark mass, the fraction of right-handed W^+-bosons would still be small, suppressed by a factor of m_b^2/m_t^2. The fractions F_i then turn out to be [13, 19]:

$$F_0 = 0.698 \pm (0.01 - 0.02)$$
$$F_- = 0.301 \pm (0.01 - 0.02)$$
$$F_+ = 4.1 \cdot 10^{-4} \pm \mathcal{O}(10^{-3})$$

These values are calculated assuming the masses $m_t = (173.3 \pm 1.1)$ GeV/c^2, $m_W = (80.399 \pm 0.023)$ GeV/c^2 and $m_b = 5$ GeV/c^2 for the top quark, W-boson and b-quark, respectively [1, 2]. Measuring a significant fraction of right-handed W-bosons would be a hint towards physics that cannot be described by the SM.
There are several different methods to analyse the helicity fractions of the W in top quark decays. A popular method is determining the helicity fractions via $\cos\theta^*$, where the angle θ^* is defined as the angle between the charged lepton and the top quark in the rest frame of the W-boson. Another way of determining the fractions is via the transverse momentum, p_{T}, of the charged lepton whose spectrum differs according to the helicity state of the W-boson. Another discriminant is the invariant mass $M_{\ell b}^2$ of lepton and b-quark which is closely related to $\cos\theta^*$. All these methods have different major sources for systematic uncertainties concerning the determination from data. Combining these methods provides a possibility to decrease the overall systematic uncertainties on the helicity measurement.

2.4.1. Experimental Status

Until 2011 the W-helicity fractions have been studied at the Tevatron collider only. The newest measurements using data from the Atlas detector are presented in [19]. There the helicity fractions are determined with the analysis of the $\cos\theta^*$ distribution via the template method. Three templates for the different helicity states and one template for the

background are used. The background template contains a data-driven QCD multijet-production estimate and contributions from single top, diboson, Z+jets and W+jets events computed from Monte Carlo simulations. The measured W-helicity fractions are:

$$F_0 = 0.59 \pm 0.12$$
$$F_- = 0.41 \pm 0.12$$

The measurement is done in the combined e+jets and μ+jets channel with a data set corresponding to an integrated luminosity of $\int \mathcal{L} \mathrm{d}t = 35\ \mathrm{pb}^{-1}$. The right-handed fraction is assumed to be fixed to its SM expectation ($F_+ = 0$). The results are in agreement with the SM expectation values. Further measurements are planned to decrease these uncertainties.

2.5. Data-Driven Estimation of *W*+ Jets Background

Several studies have been performed towards data-driven W+jets estimates at the ATLAS experiment. Three different methods are presented in [20] and will be briefly introduced here.

The first approach used is known as *Berends-Giele scaling* [21, 22] and exploits the assumption of a constant production ratio of $W + n$ jets to $W + (n-1)$ jets as described in Sect. 2.3.1. One obtains the estimate for the number of $W+ \geq 4$ jets events ($W^{\geq 4\mathrm{jets}}$) as:

$$W^{\geq 4\mathrm{jets}} = W^{2\mathrm{jets}} \cdot \sum_{i=2}^{\infty} \left(\frac{W^{2\mathrm{jets}}}{W^{1\mathrm{jet}}} \right)^i .$$

Here $W^{2\mathrm{jets}}$ and $W^{1\mathrm{jet}}$ stand for the number of W events with exactly one jet and with two jets, respectively.

A second approach is based on a similar assumption. The idea is that the W/Z ratio is known to have smaller uncertainties than the inclusive W+jets rates and is also approximately constant with jet multiplicity, thus:

$$\frac{\left(W^{\geq 4\mathrm{jets}}/W^{1\mathrm{jet}}\right)_{data}}{\left(W^{\geq 4\mathrm{jets}}/W^{1\mathrm{jet}}\right)_{MC}} = \frac{\left(Z^{\geq 4\mathrm{jets}}/Z^{1\mathrm{jet}}\right)_{data}}{\left(Z^{\geq 4\mathrm{jets}}/Z^{1\mathrm{jet}}\right)_{MC}}.$$

Transformation of this formula leads to an estimate of $(W^{\geq 4\mathrm{jets}})_{data}$ events. The double ratios provide less sensitivity to systematic uncertainties compared to the geometric series

used for Berends-Giele scaling.
A third method makes use of the charge asymmetry in the production of W-bosons, described in Sect. 2.3.1, while the $t\bar{t}$ process is a charge symmetric process (equal production of positively and negatively charged leptons). Assuming that all other contributions to a $t\bar{t}$ event sample are charge symmetric as well (neglecting the charge asymmetry of single top production because of the low cross section) the amount of $W^{\geq 4\text{jets}}$ events can be computed as:

$$W^{\geq 4\text{jets}} = \left(\frac{r_{MC}+1}{r_{MC}-1}\right)(D^+ - D^-)$$

Here D^+ and D^- denote all events with positively and negatively charged leptons, respectively. The value $r_{MC} = \frac{\sigma(pp\to W^+)}{\sigma(pp\to W^-)}$ is evaluated using MC simulations for the signal region.

All three methods are based on assumptions from theory and on MC predictions. An alternative approach that is used in this thesis is free[6] of these assumptions. The aim is to understand the W+jets background including all jet multiplicities. This can be achieved by fitting the jet multiplicity distribution from MC to data points in a W+jets enriched sample [23]. One can then determine scale factors for individual multiplicity samples, the $W+0, W+1, W+2, W+3, W+4$ and $W+\geq 5$ partons samples. The other background contributions except for the data-driven QCD multijet production are obtained from MC calculations. The fit will be performed via the template method. The explanation of the precise procedure of this background estimate needs first of all the introduction of the required tools and MC samples. Therefore the precise description of the estimation method will be given later in Chapter 7. The required introduction of the experimental setup as well follows in the next chapter.

[6]Not completely free as almost all the analysis methods in HEP use Monte Carlo predictions.

3. Experimental Setup

The Large Hadron Collider (LHC) located at CERN (Geneva) and the ATLAS experiment in particular will be introduced in the following. Data collected by the ATLAS experiment is used in the analysis. The experimental setup of the ATLAS detector used to collect the data is described in this chapter.

3.1. The Large Hadron Collider

The LHC is a proton-proton collider which was originally designed to run at a center-of-mass energy of $\sqrt{s} = 14$ TeV and a luminosity of $\mathcal{L} = 10^{34}\ \mathrm{cm}^{-2}\mathrm{s}^{-1}$ which shall enable about 40 million collisions per second. The collider is currently running at a center-of-mass energy of $\sqrt{s} = 7$ TeV and a peak stable luminosity of $\mathcal{L} = 1.26 \cdot 10^{33}\ \mathrm{cm}^{-2}\mathrm{s}^{-1}$ [24]. Therefore the LHC achieves event rates that exceed significantly the event rates of other colliders. The huge event rates enable more precise analyses with more precise estimates of background processes due to decreased statistical uncertainties on performed measurements. There are four major experiments based at the LHC: ALICE, ATLAS, CMS and LHCb. The data used in this analysis has been collected by the ATLAS detector in early 2011. The experimental setup is briefly described in the following.

3.2. The ATLAS Experiment

The ATLAS detector is a multi purpose detector and covers a wide range of particle physics aspects that are investigated at the ATLAS experiment.
With a total length of 44 m and a mass of about 7000 t, the ATLAS detector (A Toroidal LHC ApparatuS) is forward-backward symmetric with respect to the interaction point and covers nearly the entire solid angle around the collision point [25, 26]. The ATLAS detector consists of four major components: the inner detector (ID, tracking chamber), electromagnetic and hadronic calorimeters, the muon spectrometer and the magnet system containing solenoidal and toroidal magnets.

3.2.1. Coordinate System

The ATLAS detector uses a right-handed cartesian coordinate system with x-, y- und z-axis and the origin in the interaction point. The z-axis points along the beam-pipe while the x-axis points towards the center of the LHC ring and the y-axis vertically upwards. The $x-y$-plane is called the transverse plane in which the azimuthal angle ϕ is measured. The polar angle which lies between the momentum of a particle and the z-axis is denoted by θ. The transverse momentum and transverse energy are defined as $p_{\mathrm{T}} = p \sin\theta$ and $E_{\mathrm{T}} = E \sin\theta$, where $p = \sqrt{p_x^2 + p_y^2 + p_z^2}$ is the magnitude of the measured momentum and E the total energy measured.
The introduction of the so-called pseudorapidity η is also helpful:

$$\eta = -\ln\left(\tan\left(\frac{\theta}{2}\right)\right).$$

The different components of the detector cover different regions of η. The advantage of using the pseudorapidity is the invariance of $\Delta\eta$ under Lorentz boosts along the beam-line. Distances between particles are expressed by ΔR:

$$\Delta R = \sqrt{\Delta\eta^2 + \Delta\phi^2}.$$

3.2.2. The Inner Detector

The inner detector is surrounded by a solenoidal magnet that provides 2 T axial magnetic field. The ID covers the full azimuthal angle ϕ and consists of the *pixel detector*, the *silicon microstrip tracker* (*semiconductor tracker* SCT) and the *transition radiation tracker* (TRT). The first two components provide tracking of charged particles in the range of $|\eta| < 2.5$, the last one in the range of $|\eta| < 2.0$.
The pixel detector consists of three layers with high granularity and about 80.4 million readout channels and covers the vertex[1] region. It provides typically three measurements per track whereas the silicon microstrip tracker provides four measurements from eight strip layers per track. The SCT contains 6.3 million readout channels and enables determination of the vertex position. The TRT enables extended track reconstruction via more than 30 straw-tubes, which are filled with gas (70% Xenon, 27% CO_2, 3% O_2) and measure the drift time of a charge after ionization caused by charged particles. Placed at the

[1]The vertex is the point of interaction.

outer radius of the ID the TRT provides significant momentum resolution due to a larger number of measurements and a larger measured track length. It also provides additional electron identification information by the detection of transition-radiation photons in the gas mixture of the straw tubes.

3.2.3. The Calorimeters

Calorimeters are used to measure the energy E of particles that pass through the detector. Sampling calorimeters consist of a passive absorber material where interactions take place and an active material that can process signals of traversing particles. These two components are arranged in alternating layers.
If electrons or photons enter the electromagnetic (EM) calorimeter they produce secondary particles through e^+e^- pair-production and Bremsstrahlung due to the interaction with the passive absorber. The secondary particles themselves produce other particles, which leads to a shower of particles. This shower is stopped when the energy of the particles is too low to produce other particles. The measured energy is proportional to the number N of particles in the shower which follow Poissonian statistics. The energy resolution of a calorimeter is:

$$\frac{\sigma_E}{E} \propto \frac{1}{\sqrt{N}} \quad \Rightarrow \quad \frac{\sigma_E}{E} = \frac{a}{\sqrt{E}} \oplus b$$

Here a is a factor that depends on the used material and the structure of the calorimeter. The operator $\oplus$ means that a certain value, b, has to be added as systematic uncertainty (in quadrature) due to miscalibration, noise, lost energy etc. [12].
The calorimeters consist of cells. Energy deposition in adjacent cells are called 'clusters'. At the ATLAS experiment, sampling calorimeters are used for both electromagnetic and hadronic calorimeters. The calorimeter system is divided into barrel and two end-cap components plus forward calorimeters.
The EM calorimeter is a lead and liquid Argon (LAr) sampling calorimeter with accordion-shaped Kapton electrodes and covers the region $|\eta| < 3.2$ in pseudorapidity (both barrel and end-cap). An additional forward electromagnetic copper/LAr calorimeter covers the region with $3.2 < |\eta| < 4.9$.
The hadronic calorimeter is composed of a scintillating tile calorimeter which uses steel as absorber material ($|\eta| < 1.7$) and a lead LAr sampling calorimeter in the end-cap, which covers the region $1.5 < |\eta| < 3.2$. In addition, a hadronic tungsten/LAr calorimeter covers the forward region $3.2 < |\eta| < 4.9$.

3.2.4. The Muon Spectrometer

The muon system is the outer part of the ATLAS detector and consists of four different types of detectors and covers the region $|\eta| < 2.7$ in pseudorapidity. The momentum measurement of the muons is based on high precision tracking of the *monitored drift tubes* and the *cathode strip chambers*. The bending of tracks in the muon system is provided by an additional toroid magnet system which consists of three large superconducting, air-cored toroids arranged with an eight-fold azimuthal coil symmetry around the calorimeters.
The other two detectors, the *thin gap chambers* and the *resistive plate chambers* are used in the trigger system.

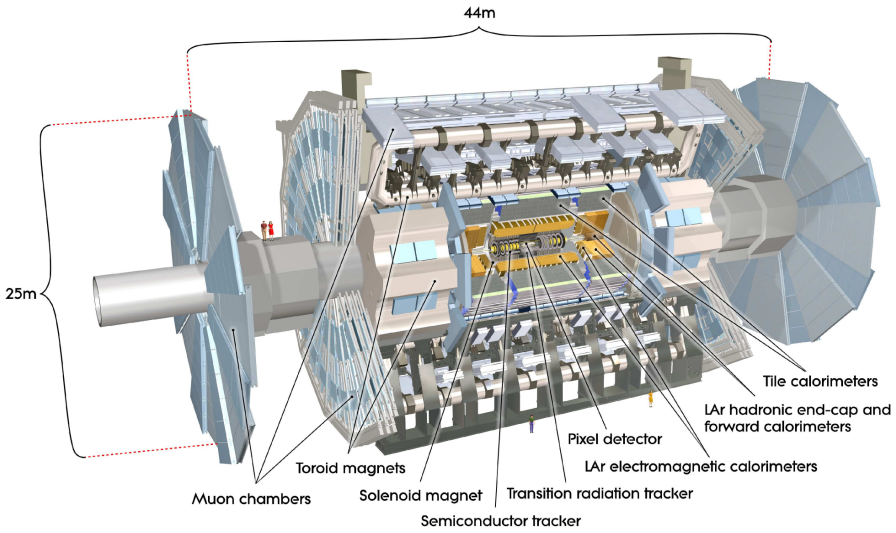

Figure 3.1.: Sketch of the ATLAS detector

Figure 3.1 shows a cut-away view of the ATLAS detector with the positions of the individual components shortly described here. The aimed resolutions of the different detector components are summarized in Table 3.1. While the tracking resolution improves with decreasing momentum, the resolution of the calorimeters improves with higher energy of a particle.

3.2.5. The Trigger system

The high luminosity at the LHC leads to a huge amount of data. In order to store only the data of interest, a three level trigger system is used within ATLAS. The Level 1 trigger is hardware based and uses a subset of the full detector information to reduce the rates from 45 MHz down to 75 kHz. It looks at high transverse momentum electrons,

Detector Component	Required Resolution
Tracking (ID)	$\sigma_{p_\mathrm{T}}/p_\mathrm{T} = 0.05\% p_\mathrm{T} \oplus 1\%$
EM calorimetry	$\sigma_E/E = 10\%/\sqrt{E} \oplus 0.7\%$
Hadronic calorimetry:	
barrel and end-cap	$\sigma_E/E = 50\%/\sqrt{E} \oplus 3\%$
forward	$\sigma_E/E = 100\%/\sqrt{E} \oplus 10\%$
Muon spectrometer	$\sigma_{p_\mathrm{T}}/p_\mathrm{T} = 10\%$ at $p_\mathrm{T} = 1$ TeV/c

Table 3.1.: Performance goals of the different detector components. The units for E and p_T are in GeV and GeV/c, respectively [25].

muons, photons, jets and hadronically decaying τ leptons as well as for large $\not{E}_T$ and total transverse energy. The Level 1 trigger then defines Regions-of-Interest (ROI) via η and ϕ coordinates and passes the information to the Level 2 trigger. The Level 2 trigger then checks these ROI and puts together the information from all detector components to reconstruct the event. After that events are sent to the Event Filter farm which reconstructs and analyses the data with high precision algorithms. The Level 2 and the Event Filter trigger are called high level trigger. They are software based and reduce the data acquisition rate finally to 200 Hz.

4. Monte Carlo Simulation

This chapter deals with the Monte Carlo (MC) simulations in general and with generators used in the analysis in particular. Monte Carlo simulations are crucial for every HEP analysis as they provide a possibility to correct measured data for detector effects, to compare the data with theory and to test the analysis tools and make closure tests.

In general, a Monte Carlo simulation is a method of determining properties of certain models by using iterative sampling. This means that the MC simulation repeatedly generates random numbers that are used as input variables. With this input, a MC generator produces a large number of possible outcomes with respect to the model, described by a certain probability distribution. This is especially used for models with significant uncertainty on the input variables and systems with a large number of coupled degrees of freedom.
The purpose in most of particle physics experiments is to simulate events that are produced in collision experiments and measured in a detector. This is done by event generators which produce randomly possible events with a frequency distribution predicted by theory [27]. For example, concerning the modeling of hard processes, event generators produce events by phase space sampling. The phase space is a multi-dimensional hypercube which spans all of the degrees of freedom.
Often different event generators are used to produce a single event. These different generators are specialized on processes like hard processes, parton showering or hadronization. In the next section the used MC samples for the different relevant processes and the compositions of different generators are described.

4.1. Monte Carlo Samples

A variety of MC generators is used in this analysis. All MC samples are generated with a center-of-mass energy of $\sqrt{s} = 7$ TeV in proton-proton collisions. The ATLAS detector simulation is performed with the GEANT4 toolkit [28].
For the W+jets samples, the MC generator ALPGEN [29] is used. ALPGEN is a generator

that simulates multiparton hard processes in hadronic collisions in LO QCD and electroweak interactions.
ALPGEN provides the complete parton-level simulation via the calculation of the LO matrix elements (ME) and offers the possibility to carry out hadronization of the partonic final state, thus *parton showering* (PS). Showering is done via considering the probability of a quark to emit a gluon. While the ME enables an accurate description of hard processes on parton level, the PS gives a realistic description of the final state on hadron level. The used samples are W+N partons with N$\in$(0,..,5). The showering is done with HERWIG [30] and the underlying events is modeled using JIMMY [31]. The Np5 sample is an inclusive multiplicity sample, including five and more partons. The term 'parton' describes a single quark or gluon without taking into account fragmentation and hadronization effects or the radiation of a gluon. Therefore, the jet multiplicity differs from the parton multiplicity. The numbers of partons are not necessarily equal to the number of jets because there is the possibility that one can loose a jet or measure an additional jet in the detector due to imperfect jet reconstruction and limited detector acceptance.
As just mentioned the ME calculation and the PS are different complementary processes that have to be combined to form a certain multiplicity sample. The problem then is that certain final states can arise both in a $W + n$ partons sample that has not received an extra jet via PS and a $W + n - 1$ partons sample that receives an additional jet through PS, which would lead to double-counting. To avoid double-counting 'MLM' matching is used within ALPGEN. The matching of ME partons and PS jets is done with a certain requirement for ΔR (< 0.7) of parton and jet, where a jet can only be matched to one parton [29, 32]. The event is rejected if not all partons are matched to a jet. If there are additional unmatched jets which are softer than the ME partons, the event is kept for an inclusive multiplicity sample.
In addition to the W+Np samples $Wb\bar{b}$+jets, $Wc\bar{c}$+jets and Wc+jets are used that will play a certain role in terms of the heavy flavour treatment (see Section 7.1). The Tables A.1-A.3 in Appendix A give an overview of all mentioned samples and the other background samples, in this case for the processes $t\bar{t}$, single top, Z+jets and diboson, used for the analysis. For the processes containing top quarks ($t\bar{t}$ and single top) the generator MC@NLO [33] is used which includes next-to-leading order QCD corrections in the simulation of hard processes. For diboson processes HERWIG [30] is used, which is a general purpose MC event generator that includes hard scattering processes, initial- and final-state radiation through parton showering, hadronization and hadron decays and underlying event simulation.

5. Event Reconstruction

This chapter gives an overview of the criteria used to extract the relevant information from MC and data to be used in the analysis. First, the object definitions are introduced, followed by the description of the event selection of a W+jets enriched sample. The object definitions and event selections are later on applied to both MC samples and data samples in order to get a good description of data with the simulated samples.

5.1. Object Definition

The reconstruction of $t\bar{t}$ events and W+jets events makes use of the whole ATLAS detector described in Section 3.2. The detector components therefore have to be fully operational in terms of the data samples that will be used for the analysis. The objects relevant for the analysis have to be defined first. The term "object" comprises muons, electrons, jets and $\not{E}_T$ as an indicator of undetected neutrinos.
Electrons are reconstructed from electromagnetic clusters via the "sliding window" algorithm and finally matching of tracks in ID and cluster [34]. The requirements are:

- the pseudorapidity has to be in the region of $|\eta_{cluster}| = |\eta| < 2.47$
- the transition region between barrel and end-cap calorimeters is excluded ("crack region": $1.37 < 7 < |\eta| < 1.52$)
- the minimum transverse momentum is 25 GeV/c

The electron is required to be isolated. Therefore, the additional transverse energy that is allowed to be in a cone of $\Delta R = 0.3$ around the electron has to be smaller than 3.5 GeV. This additional energy is corrected for leakage and pileup effects[1].
A muon is reconstructed via matching of hits in the ID and the muon spectrometer. The

[1]Pileup denotes multi-interactions in one or consecutive bunch crossings, that are counted as one event. The MC predictions have to be reweighted due to pileup effects. The average number of reconstructed vertices in a event gives a measure for this reweighting.

requirements for tight muons are:

- $p_{\mathrm{T}} > 20$ GeV
- $|\eta_{\mathrm{max}}| < 2.5$
- isolation criteria: ptcone30 < 4 GeV/c and etcone30 < 4 GeV
- overlap radius of $\Delta R = 0.4$: If jets are within this cone, the muon is likely to be emitted from a jet. The muon is not considered further in this analysis.
- furthermore certain track criteria have to be fulfilled, see [35]

The denotations ptcone30 < 4 GeV/c and etcone30 < 4 GeV for the muon isolation stand for the requirements of no larger transverse momentum measurement than 4 GeV/c and no larger transverse energy deposition than 4 GeV in a cone of $\Delta R = 0.3$ around the muon direction, respectively.
Jets reconstructed via the anti-k_{T} algorithm [36], have to fulfill $|\eta_{\mathrm{max}}| < 2.5$. They are considered to be a mis-identified electron if they are within $\Delta R = 0.2$ of a well reconstructed electron.

5.2. Event Selection

The goal of the analysis is to get a data-driven W+jets estimate for a $t\bar{t}$-analysis. This can be done in a W+jets enriched sample. For the following studies, the term "background" is used in the meaning of background processes for the W+jets enriched selection, containing $t\bar{t}$, single top, Z+jets, diboson and multijet production.
The criteria for the W+jets enriched selection follow in Section 5.2.1.

5.2.1. *W*+Jets Enriched

The W+jets enriched sample is obtained by applying the following selection criteria, described in [23], which differ from the standard $t\bar{t}$ event selection. The requirements are:

- exactly one lepton with $p_{\mathrm{T}} > 20$ GeV/c
- the lepton has fired the trigger (including trigger matching)

- veto on the presence of any other lepton with $p_{\mathrm{T}} > 10$ GeV/c
- jet $p_{\mathrm{T}} > 25$ GeV/c
- 30 GeV$< \not{E}_T <$ 80 GeV
- 40 GeV/$c^2 < m_{\mathrm{T}}(W) <$80 GeV/$c^2$, [2]
- veto on events in which one of the four hardest jets is b-tagged

In this selection b-tagging information is used. The b-tagging algorithm applied is the $SV0$ algorithm that makes use of the relatively long lifetime of hadrons containing b-quarks. A secondary vertex can be reconstructed that provides information used for the b-tagging weight. If the b-tagging weight exceeds 5.85 a jet is counted as a b-jet with a tagging efficiency of 50% [37].

5.2.2. Corrections to Simulated Samples

In order to correct the MC distribution to match the data, several aspects have to be taken into account. These corrections comprise trigger, identification and reconstruction efficiencies dependent on η and p_{T} of the leptons [35, 38] as well as taking into account the b-tagging calibration [37]. Furthermore an additional correction is necessary on the muon momentum resolution (resolution smearing in MC) to get a better description of the muon momentum distribution [39].

[2] The transverse W-boson mass is defined as $m_T(W) = \sqrt{2p_T^{\ell}\not{E}_T(1-\cos(\phi^{\ell}-\phi^{\nu}))}$.

6. Statistical Tools

Before explaining the procedure of the data-driven background estimation it is necessary to introduce the statistical tools that are used in the presented analysis. This chapter discusses the major aspects of the statistical methods of data analysis such as Bayes' Theorem and the Maximum Likelihood Method. The W+jets background estimation uses the template method that is introduced as well as the *Bayesian Analysis Toolkit* that provides the fundamental technical framework for the analysis.

6.1. Maximum Likelihood

The *Maximum Likelihood Method* is a method to estimate parameters from a given data set assuming a certain model. It can also be used for hypothesis testing but here we focus on the parameter estimation.
A set of parameters $\vec{a}$ can be estimated given a data set $\{x_1, x_2, ..., x_N\}$ with the variables x_i that are distributed according to a parent distribution (probability density function) $P(x_i; \vec{a})$. The likelihood L is then defined as the probability of a certain set of data points x_i measured in an experiment:

$$L = P(x_1, x_2, ..., x_N; \vec{a}) = \prod_i^N P(x_i; a).$$

One will find the best estimates for the parameters $\vec{a}$ by maximizing the likelihood.

6.2. Bayes' Theorem

The data set is denoted as $\vec{x}$ and a set of parameters $\vec{a}$ represents a certain model or a certain theory. The probability for the theory to be correct given a measured data set is

given by:

$$P(\vec{a} \mid \vec{x}) = \frac{P(\vec{x} \mid \vec{a}) \cdot P(\vec{a})}{P(\vec{x})} \tag{6.1}$$

This equation represents the *Bayes' Theorem*. $P(\vec{x} \mid \vec{a})$ is the introduced likelihood L, the probability to observe a specific data set for a given model. $P(\vec{a})$ and $P(\vec{x})$ denote the *prior probability densities*, in short called *priors*. $P(\vec{a} \mid \vec{x})$ is the searched quantity the so-called *posterior probability density* (*posterior*). The priors represent the knowledge before performing an experiment. They are not in any sense frequency distributions but can be seen as *degrees-of-belief*, which contain our knowledge about nature that will be updated by comparing the model with data [40]. Thus the Bayes' Theorem is a scheme for updating our knowledge. The posterior strongly depends on the choice of the priors. Applying flat priors (assuming equal probabilities in a given range) the parameter estimation using the mode of the posterior is equivalent to the Maximum Likelihood Method.
Performing the parameter estimation with the help of Bayes' Theorem can be difficult in cases of multi-dimensional spaces. The technical framework to facilitate the implementation of the method is provided by the *Bayesian Analysis Toolkit*.

6.3. The Bayesian Analysis Toolkit - BAT

The Bayesian Analysis Toolkit (BAT) is a software package that is based on Bayes' Theorem [41]. It gives access to the full posterior with the use of *Markov Chain Monte Carlo* (*MCMC*) [42] and MINUIT [43] and thus enables parameter estimation and comparisons of model predictions with data.
MINUIT is a function minimization and error analysis computer program. It is used to perform ensemble tests (see Sect. 8.4). With given start parameters it searches for global minima via the gradient method. For the actual template fit the $MCMC$ algorithm is used to find the initial values for the best estimates of the parameters. It passes these values on to MINUIT which then performs the final minimization.
Markov Chain Monte Carlo is a method whose aim is to map a positive function $\pi(z)$ by taking a random walk to points with higher probabilities. In BAT, MCMC is used to find the parameters maximizing the posterior probability. Different algorithms can be used to do so. For this analysis, the Metropolis algorithm is used. This algorithm works as follows:

- start at some randomly chosen z_i

- randomly generate y around z_i
- accept y as next step if $\pi(y)/\pi(z_i)$ exceeds some randomly generated value $U \in [0, 1]$ otherwise stay where you are, $z_{i+1} = z_i$
- start over

The parameters which maximize $P(\vec{a} \mid \vec{x})$, the global modes, are used as the estimates for the searched parameters. One can find an estimator for a single model parameter by "marginalization",

$$P(a_i \mid \vec{x}) = \int P(\vec{a} \mid \vec{x}) \prod_{j \neq i} \mathrm{d}a_j.$$

This can be seen as a projection on the axis of the individual parameters. The parameters of the global mode usually do not coincide with those that maximize the marginalized distributions.

6.4. Template Method

The parameters of interest in the W+jets background estimation are the scale factors for each parton multiplicity sample as explained in Chapter 7. These parameters are estimated using the template method. The tool to perform template fits is implemented in BAT.

We have a distribution of a variable x that is filled into a histogram with N_b bins with a bin width of Δx_j consisting of unknown contributions from different processes i. The aim is to estimate the expectation value for every single contribution to a given data set, the model parameters. The model parameters are denoted by λ_i^p where i stands for a certain process. The variable x has a probability density $f_i(x)$ for every single process. These $f_i(x)$ are estimated by frequency distributions that are obtained from Monte Carlo and are normalized to unity. These frequency distributions are referred to as *templates*. The statistical uncertainties on these distributions are assumed to be negligible. The expectation value λ_j for each bin j can be calculated as:

$$\lambda_j = \sum_i \lambda_i^p \cdot \int_{\Delta x_j} f_i(x) \mathrm{d}x$$

In BAT, fitting the given templates to a data distribution means to find the global mode of the posterior according to Equation 6.1, Bayes' Theorem [44]. One has to replace $\vec{a}$ with $\lambda_i^p, i = 1, 2, ...$ or short $\vec{\lambda^p}$. The likelihood is then defined as

$$P(\vec{x} \mid \vec{\lambda^p}) = \prod_i^{N_b} \frac{\lambda_i^{n_i}}{n_i!} \cdot \mathrm{e}^{-\lambda_i},$$

thus a product of Poisson terms (fluctuations in each bin assumed to be independent) where n_i is the number of events in bin i and $\lambda_i \hat{=} \lambda_i^p$. Due to the application of a Gaussian prior for the background template (see Chapter 7) for the template fit, the likelihood is then:

$$P(\vec{x} \mid \vec{\lambda^p}) = \mathrm{e}^{\frac{-(\lambda_{bkg}-\bar{\lambda}_{bkg})^2}{2\sigma_{bkg}^2}} \prod_i^{N_b} \frac{\lambda_i^{n_i}}{n_i!} \cdot \mathrm{e}^{-\lambda_i}.$$

The quantities $\bar{\lambda}_{bkg}$ and σ_{bkg} are the expectation value and the uncertainty on the background, respectively. The descriptions in Chapter 7 refers to the quantities introduced here and explains the exact implementation of the BAT template fitting tool in the analysis.

7. Procedure of Background Estimation

In this chapter, the precise procedure of the data-driven W+jets background estimate is described.

First, the event selection described in Sect. 5.2.1 is performed on both MC and data samples in the muon channel (μ+jets events). The data samples are taken from an integrated luminosity of $\int \mathcal{L} \mathrm{d}t = 163.4$ pb^{-1} taken by the ATLAS experiment in early 2011. The MC samples are normalized to this luminosity with respect to their production cross sections. The QCD multijet production is estimated from data using the matrix method (see Sect. 7.2). Furthermore the different efficiencies are taken into account such as trigger efficiencies, reconstruction efficiencies, b-tagging efficiencies and pile-up re-weighting (see Chapter 5. Note that in this case the b-tagging efficiency represents the probability to tag a jet as a b-jet, which is actually no b-jet (we have the selection criterion of a b-tag veto). In addition, resolution smearing on MC samples is applied to match the data resolution.

The approach used by the $t\bar{t}$ resonance group [23] is used as a baseline. In contrast to this approach, here the background containing $t\bar{t}$, diboson, Z+jets, single top events plus multijet production is not subtracted from data but taken as an additional template constrained by a Gaussian prior. The background also contains the $W+$ heavy flavour jets contribution (see Section 7.1). The templates for the fit are extracted from the MC jet multiplicity distributions. A total number of seven templates are produced for the background, W+0 partons, W+1 parton, W+2 partons, W+3 partons, W+4 partons and W+5 inclusive partons. The templates are jet multiplicity histograms for each MC sample normalized to unity. These templates are then fitted to the data histogram. The histograms consist of eight bins, thus the multiplicity up to a seven inclusive jet bin was used. The parameters for W+0 partons to W+5 inclusive partons are the total number of events per template. One obtains the ratio of $\frac{N_{\text{events}}(\text{after fit})}{N_{\text{events}}(\text{before fit})}$ called scale factor. These scale factors shall be applied to the W multiplicity samples and are a correction of MC predictions obtained by analysing the data. One has to take into account the generation of the W samples and the MLM matching that is used to combine the different multi-

plicity samples in order to get fixed fractions of these representing the inclusive W+jets process as a whole physics process (see Sect. 4.1). With respect to this matching the parameters that are obtained by the template fit are limited. Changing parameters like the jet p_{T} or other quantities in the MC generation and matching leads to deviations of the W+jets composition of the individual multiplicity samples up to 20% [45]. So the matching procedure has its own systematic uncertainties that are exploited here. The aim is not to rely too much on MC predictions but to exploit the systematic uncertainties on these predictions and correct the individual fractions of W+jets processes with measured data. Also considering the low multiplicity contributions although they are actually not background for $t\bar{t}$ events has the advantage that one can make use of the high amount of data, thus low statistical uncertainties.

The actual template fit is performed using the template fitting tool implemented in BAT [41]. Due to the fact that we have no prior knowledge of the scale factors for the $W+n$ partons samples flat priors are used. The background template is allowed to fluctuate around its MC expectation value with its uncertainty, thus the prior is constrained to a Gaussian with the mean of the MC expectation value and the statistical uncertainty of this value ($\sqrt{N}$) as the width.

7.1. Heavy Flavour Treatment

In the analysis, events with a W and b or c quarks, denoted as $W+$ heavy flavour, are treated separately from the rest of the W+jets events.
This separate treatment is necessary because of the different selection efficiencies of light and heavy flavour samples due to the b-tag veto in the W+jets enriched selection that is actually a $W+$ light jets enriched selection. This selection is therefore orthogonal to the $t\bar{t}$-selection where there is a requirement of at least one b-tag.
The Alpgen samples W+Np0 to W+Np5 are considered as $W+$ light jets samples because they are generated with light quarks u, d, s and c from the matrix element (all treated as massless). Heavy flavour quarks are added to these samples via parton showering. The samples $Wb\bar{b}$+jets, $Wc\bar{c}$+jets and Wc+jets are generated with massive b and c quarks via the matrix element. In contrast to the MLM matching for combining ME partons with PS jets there is no attempt in Alpgen to match the heavy flavour samples with the light flavour samples. It is possible that the same final states might arise e. g. in both W+Np2 and Wc+Np1 and therefore one needs to avoid double-counting. The removal of certain events is necessary and is provided by the heavy flavour overlap

removal tool (HFOR) that is described in [46]. This tool provides information of the content of light jets, $b\bar{b}, c\bar{c}$ and c and events that show up in more than one sample. This information is used in the analysis to allocate the events with heavy flavour content to the correct process, and hence to the right template. It enables the separate treatment of $W+$ heavy flavour as needed. In our case the $W+$ heavy flavour contribution is treated as a background process. Therefore, we do not obtain a single scale factor for it, only for the $W+$ light jets samples. The selection of a $W+$ light jets enriched sample does not allow for the determination of a scale factor for the $W+$ heavy flavour samples, because of the b-tag veto. A possibility to obtain a scale factor for $W+$ heavy flavour is to change the event selection in the sense that one requires a b-tag instead of vetoing it. In order to reject $t\bar{t}$ events one could then apply a jet multiplicity cut that rejects events with four jets and more (where the $t\bar{t}$-selection requires at least four jets). Then a template fit might allow for the determination of a scale factor for $W+$ heavy flavour.

7.2. Data-driven QCD Estimate

QCD multijet production events enter the selected sample via misidentified muons or misreconstruction of non prompt muons originating from a jet as prompt muons. The matrix method [47] exploits different muon identification properties between 'real' muons (isolated, originating from W and Z decays) and 'fake' muons (misidentified or non prompt). Two samples are defined after requiring the selection criteria, which only differ in the recommended muon identification criteria of 'loose' and 'tight'. The assumption is then, that the numbers of events for the different samples N_{loose} and N_{tight} can be written as follows:

$$\begin{aligned} N_{\text{loose}} &= N_{\text{real}}^{\text{loose}} + N_{\text{fake}}^{\text{loose}} \\ N_{\text{tight}} &= \epsilon_{\text{real}} N_{\text{real}}^{\text{loose}} + \epsilon_{\text{fake}} N_{\text{fake}}^{\text{loose}} \end{aligned} \tag{7.1}$$

In this system of equations $N_{\text{real}}^{\text{loose}}$ and $N_{\text{fake}}^{\text{loose}}$ represent the fractions of real and fake muons in the loose sample, respectively. ϵ_{real} and ϵ_{fake} stand for the probabilities of a real or a fake muon to also fulfill the tight selection criteria. These probabilities can be estimated using control samples. The system of equations in Eq. 7.1 then can be solved for $\epsilon_{\text{fake}} N_{\text{fake}}^{\text{loose}}$ which gives the number of events with fake muons that enter the selected sample, thus the number of events of the QCD multijet production.
For this analysis the QCD multijet production is estimated by subtracting the yields in a pretag (no requirement of b-tag) sample and a tagged sample due to the b-tag veto applied

in the selection.

8. Results

In this chapter the results of the analysis are summarized. The results of the template fits conducted to a pseudo-data sample of a W+jets enriched selection are presented. The validation of the template method used to find the scale factors for the W multiplicity samples is performed via ensemble testing. The procedure of the validation is explained in Sect. 8.4. Statistical uncertainties are evaluated. The MC-data agreement is compared before applying the scale factors and after applying the scale factors.

8.1. Comparison of Data and MC

In order to compare the selected data and MC samples, the MC samples are normalized to the luminosity of the collected data. The different contributions of the MC events have to be weighted. The event weight EW for the contributions is obtained by:

$$EW = \varepsilon \cdot \sigma \cdot k \cdot \int \mathcal{L} \mathrm{d}t \cdot SF$$

Here the integrated luminosity corresponds to the luminosity of the data. The cross sections σ for the different processes can be found in Tables A.1-A.3 in Appendix A. The selection efficiency ε is the number of selected events in a sample divided by the number of total events in the sample before the event selection. The uncertainty on ε is binominal. The k-factor is applied to match the generated events to the same order of processes (next-to-leading order NLO, or next-to-next-to leading order NNLO). SF denotes the factor that is composed of trigger-, reconstruction- and b-tagging efficiency and pileup weight. After applying the event weight to the contributions the MC expectation values for those can be calculated. The uncertainties on these values comprise the uncertainties on the luminosity (4.5% at present), the cross sections, the selection efficiency and on SF.

8.2. *W*+Jets Enriched Selection

The event yields for the W+jets enriched selection are quoted in Table 8.1. One can observe that the the total number of events for the data and the total number of events for the MC plus QCD estimate yields are not in agreement within 1σ.

μ+jets channel		
Process	$N_{est.}$	Uncert. $N_{est.}$
Ttbar (MC)	225.352	16.934
Wjets (hf) (MC)	13271.4	138.4
W+0p (MC)	286816	424
W+1p (MC)	41241	1103
W+2p (MC)	10156.7	390.8
W+3p (MC)	2380.34	103.67
W+4p (MC)	525.512	26.162
W+5p (MC)	122.863	6.296
Zjets (MC)	12296.5	204.3
Single Top (MC)	168.42	12.22
Diboson (MC)	288.007	12.850
QCD (DD)	1679.56	1679.56
Total	369172	1742
Data	372581	

Table 8.1.: Obtained expectation values from MC and uncertainties in W+jets enriched selection.

8.2.1. Control Plots

Control plots of different distributions showing MC contributions and the data points in one histogram with the Data/MC ratio are depicted in Fig. 8.1. The disagreement between the numbers for data and MC events is confirmed by these control plots. The jet multiplicity in the seventh jet-bin shows a large discrepancy between MC and data points (see Fig. 8.2). For the jet ϕ distribution it is obvious that there are problems with the MC normalization to the data, since the data-points always exceed the MC expectations. This is a observation that needs further studies to be explained. Because of these discrepancies it is not sensible to perform the template fit to the data.

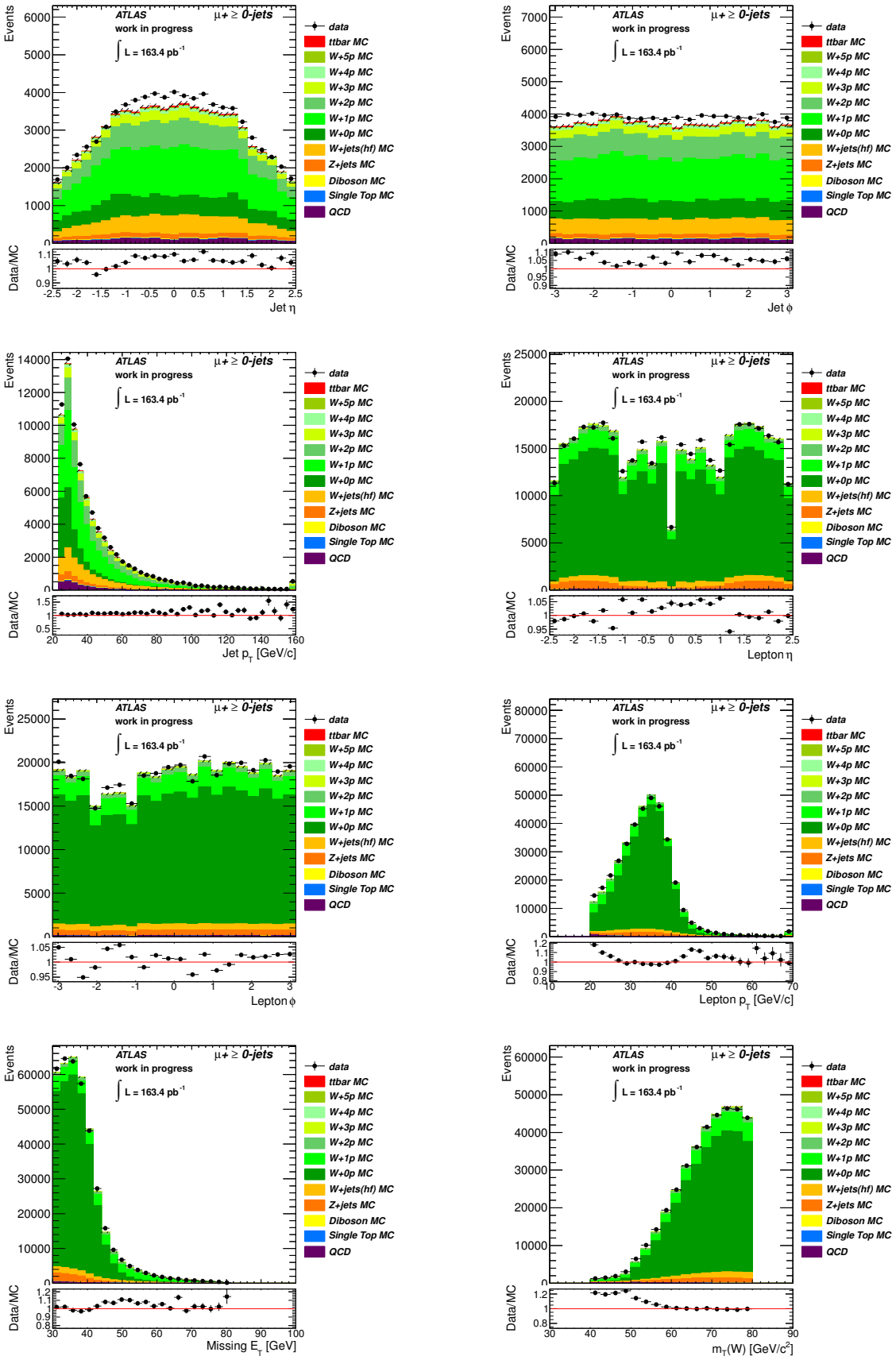

Figure 8.1.: Control Plots for jet distributions, lepton distributions, $\not{E}_T$ and transverse mass $m_{\mathrm{T}}(W)$.

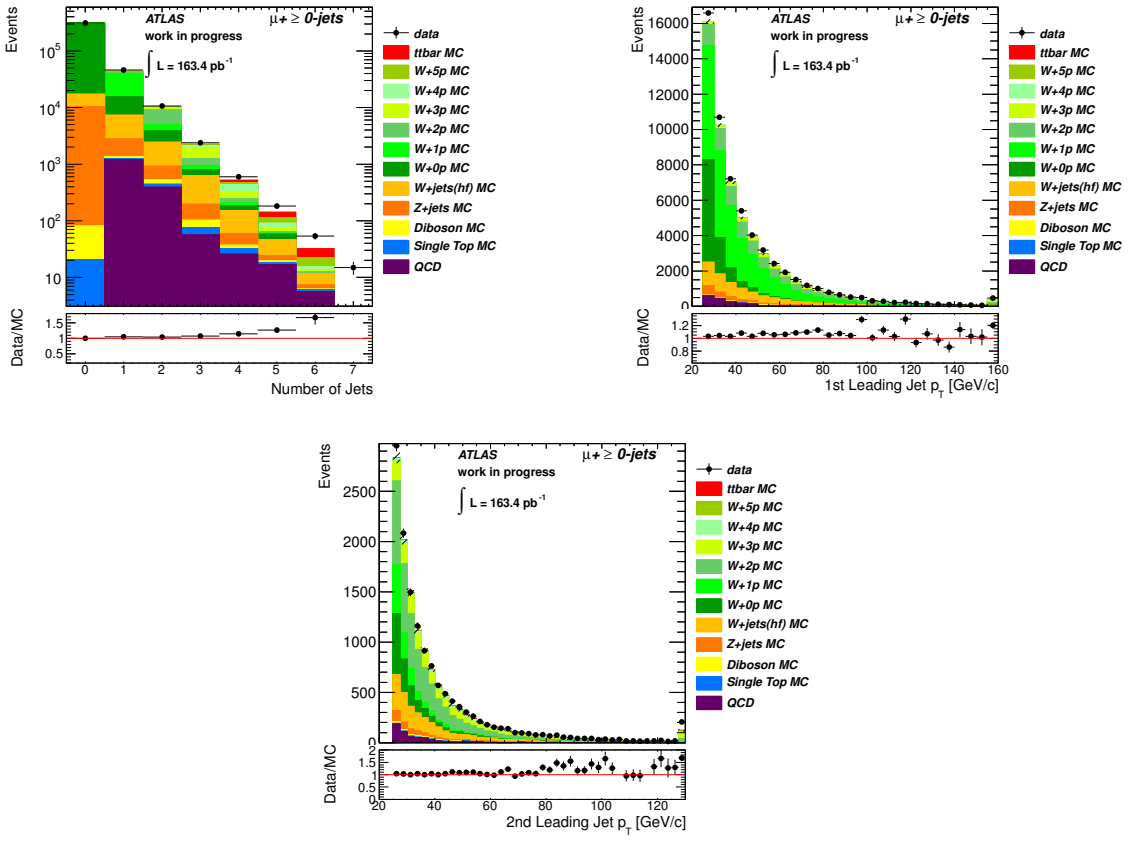

Figure 8.2.: Control plots for jet multiplicity, leading jet p_{T} and second leading jet p_{T}.

8.3. Templates

Seven templates in total are created (see Chapt. 7). All templates are normalized to unity. The templates are depicted in Fig. 8.3. The W multiplicity templates W+Np0 and W+Np1 show distinct peaks in jet bins that correspond to the number of partons with which the samples were generated. The higher multiplicity templates have peaks in the lower jet bin compared to their numbers of partons.

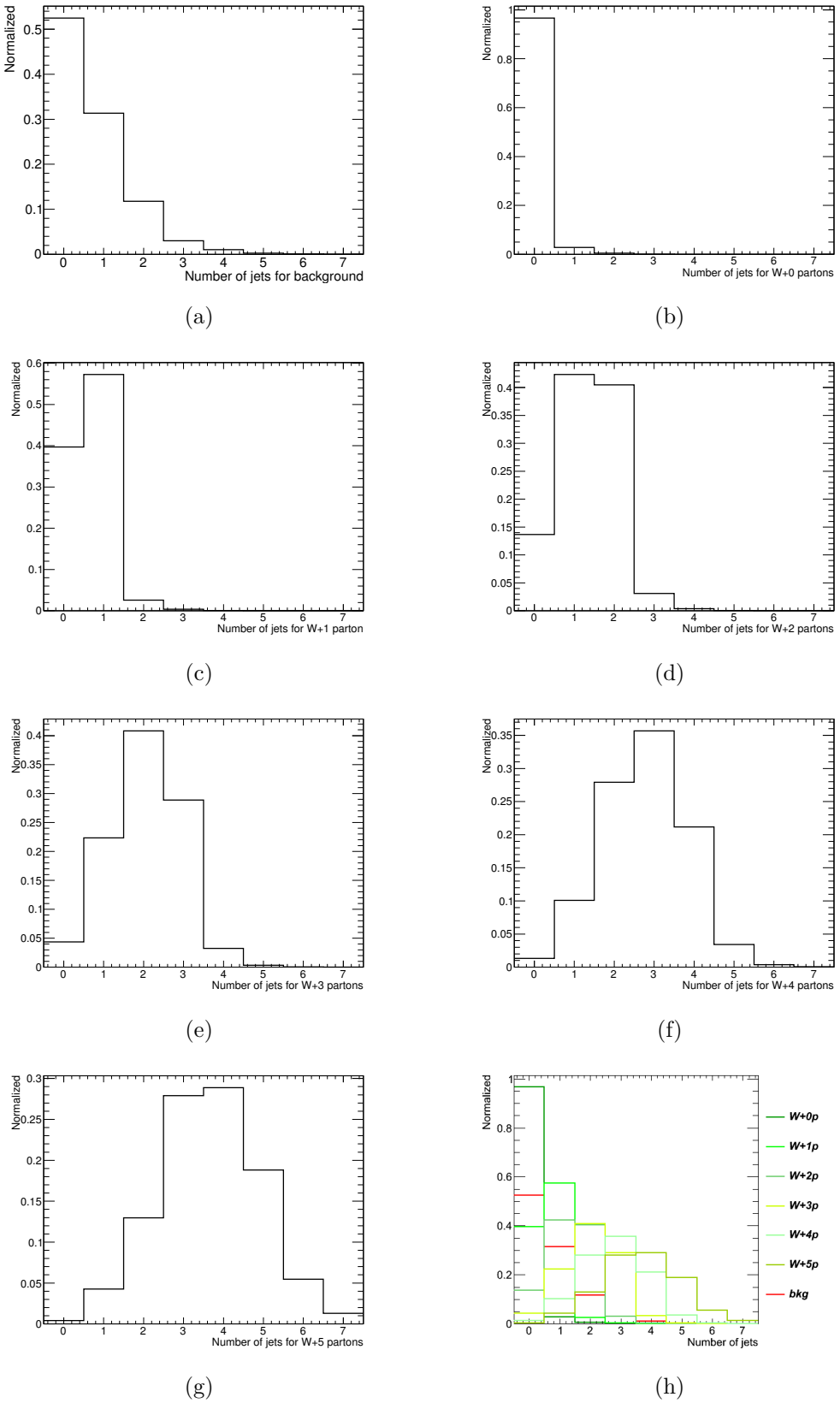

Figure 8.3.: The normalized templates of the background (a) and W+Np samples (b-g). All templates are depicted in one histogram in (h).

8.4. Ensemble Tests

The validation of the template fitting method is done by performing ensemble tests. Ensembles are created by fluctuating the single bin contents of the histogram according to a Poisson distribution. The bin contents fluctuate independently which means that the total number of entries in the histogram is also varying. The histograms that are fitted are created with different scale factors for the W multiplicity samples and are referred to as pseudo-data histograms. For each pseudo-data histogram ensemble tests are performed with 5000 ensembles each. Then, template fits to these ensembles are performed and the resulting parameter and error distributions are histogrammed. In total 54 pseudo-data histograms are created. For each multiplicity sample nine different pseudo-data sets are obtained by changing the scale factors of the multiplicity sample from 0.75 to 1.15 in 0.05 steps for WNp0 and WNp1 and from 0.6 to 1.4 in 0.1 steps for the other multiplicities. The background contribution stays the same for all pseudo-data histograms. The other multiplicity samples are scaled in order to keep the total number of entries constant. This means that the integrals of every pseudo-data histogram are equal. The range for the WNp0 and WNp1 scale factors is smaller than the others because of the larger amount of entries in these templates. All ensemble tests are conducted allowing negative parameter values, thus setting no physical constraints to the template fit.

8.4.1. Calibration Curves

Calibration curves for each W multiplicity sample are obtained by plotting the fitted scale factors (output scale factors) as a function of the input scale factors for the pseudo-data histograms. The output scale factors are calculated by taking the mean of the parameter distributions from the ensemble test and dividing it by the MC expectation value. The uncertainty on the output scale factors are obtained by error propagation of the mean error of the parameter distribution and is statistical only. The calibration curves for each W template are shown in Fig.8.4. All curves show slopes consistent with one and an offset that is consistent with zero within 1σ. Thus the calibration curves show that the fit is unbiased.

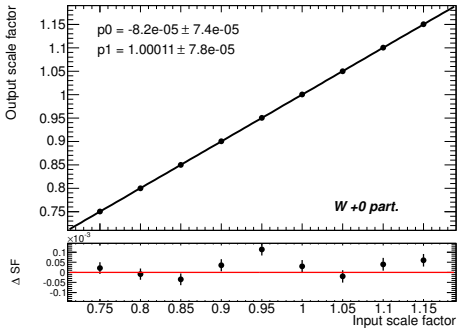

(a) W+0 partons

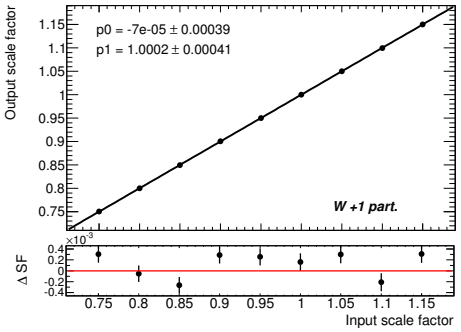

(b) W+1 parton

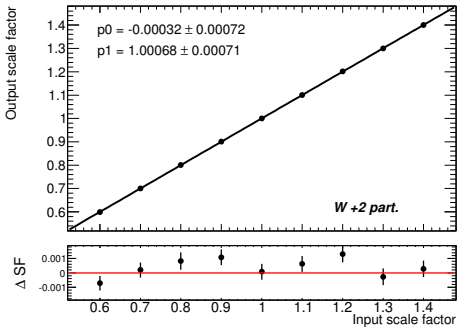

(c) W+2 partons

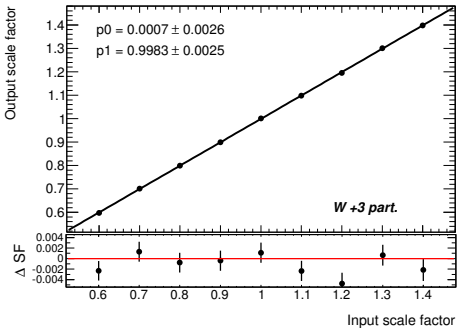

(d) W+3 partons

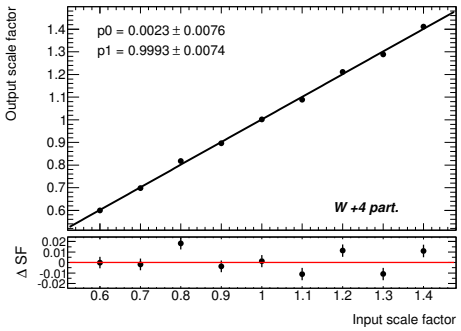

(e) W+4 partons

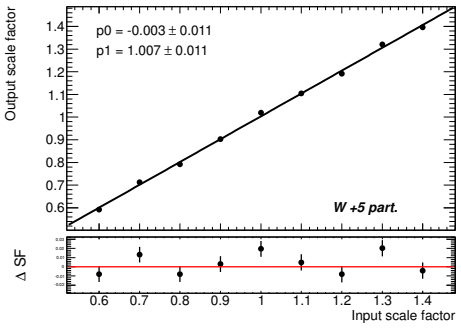

(f) W+5 partons

Figure 8.4.: Calibration curves for the different parton multiplicity samples.

8.4.2. Pull Distributions

A further check of the validity of the template fit is to draw the pull distributions. The pull distribution is defined as:

$$p_i = \frac{y_i - y_{\text{exp}}}{\sigma_i}$$

Here y_i denotes the output parameter belonging to the ith ensemble test where σ_i is the uncertainty belonging to this parameter. y_{exp} is the expected value for the fit parameter with respect to the pseudo-data histogram (input value). The pull distributions are expected to be Gaussian distributions with a mean of zero and a width (sigma) of one. Examples for these pull distributions are shown in Fig. B.1, App. B. Not all pull distributions show the behaviour of having a mean that is consistent with zero and a width that is consistent with one. Figures B.2 and B.3 in Appendix B show plots with the means and sigmas of the pull distributions as a function of the input scale factor to study the behaviour.
The conclusion is that the pull distributions are not all perfect, but the majority of the pull distributions have means and sigmas that are consistent with zero and one within 2σ, respectively.

8.5. Template Fit to Pseudo-Data

After validation of the fitting method the template fit has been performed to pseudo-data. The pseudo-data was generated by randomly choosing scale factors for the W multiplicity samples in a range of 0.8 to 1.3 and keeping the background the same with a scale factor of one. The output value of the fit is the number of entries in the individual templates. The scale factors are obtained by dividing this output value by the MC expectation value. The uncertainties on the calculated scale factors include the uncertainty on the output value and are statistical only.
The results of the fit with W+jets enriched templates to pseudo-data are quoted in Table 8.2.
The jet multiplicity distribution before and after the fit is shown in Figure 8.5.

Template	Input	Fit Output	stat. Uncertainty
background	1.00000	1.00000	0.00599
W+0partons	0.89235	0.89220	0.00206
W+1parton	1.01284	1.01282	0.01104
W+2partons	1.19653	1.19626	0.03739
W+3partons	0.940829	0.93978	0.12940
W+4partons	1.29848	1.29911	0.38059
W+5partons	0.90764	0.90751	0.58765

Table 8.2.: Results for fitted scale factors in comparison with input scale factors (W+jets enriched).

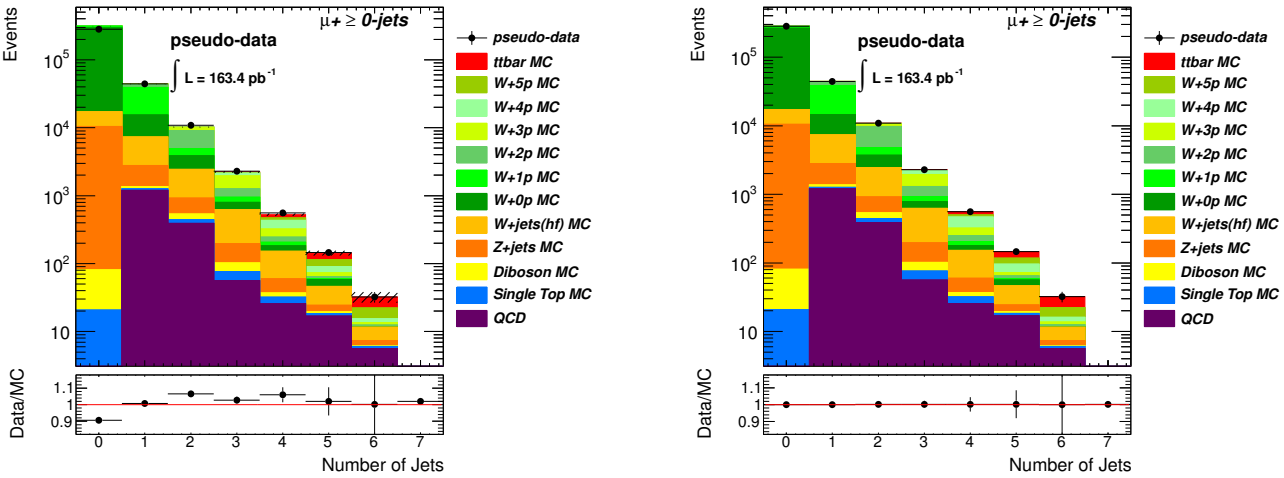

(a) before fit

(b) after fit

Figure 8.5.: Comparison of jet multiplicity distribution before (a) and after (b) applying the scale factors.

8.6. Comparison of Pre- and Post-Fit Distributions

The distributions other than the fitted jet multiplicity distribution, and the ratios for the MC and pseudo-data are compared before applying the scale factors and after applying them. Some of these distributions are depicted in Figure 8.6. One can observe a significant improvement of the Data-MC agreement, as expected. Other comparison plots can be found in the Appendix C, Fig. C.1 and Fig. C.2.

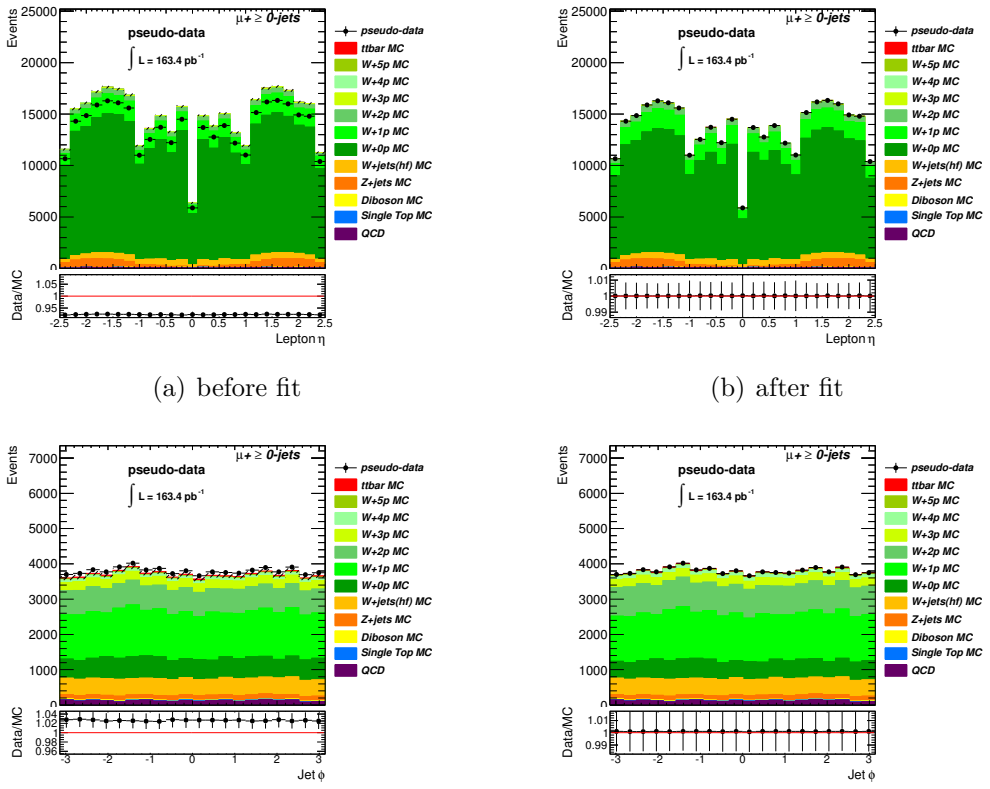

(a) before fit

(b) after fit

(c) before fit

(d) after fit

Figure 8.6.: Comparison of distributions before and after applying the fitted scale factors.

8.7. Uncertainties

8.7.1. Statistical Uncertainties

The statistical uncertainties are obtained from ensemble tests with 5000 ensembles each. Performing an ensemble test for the fit to the pseudo-data points provides a distribution of the statistical uncertainty for each parameter. The distributions for each scale factor are depicted in Fig. 8.7. One observes that the uncertainties on the single pseudo-data fit lie in the region of the means of the uncertainty distributions.
Conducting error propagation leads to the uncertainties on the scale factors which are quoted in Table 8.2.

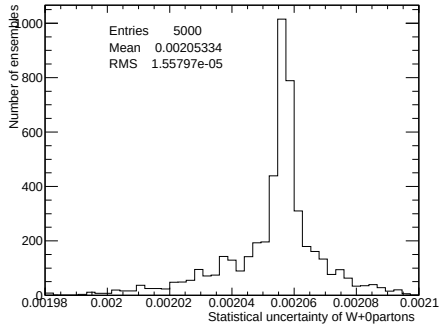

(a) W+0 partons

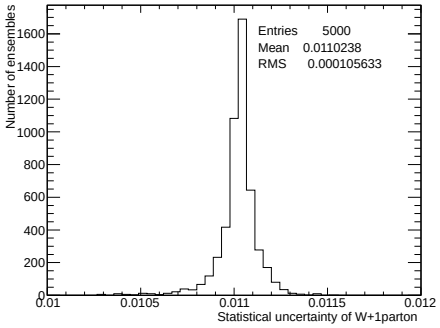

(b) W+1 parton

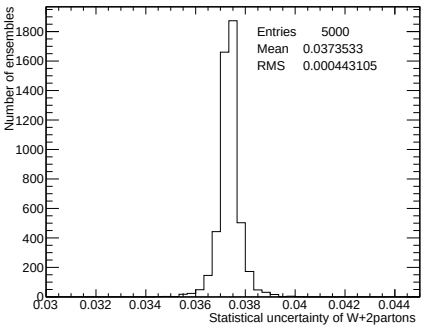

(c) W+2 partons

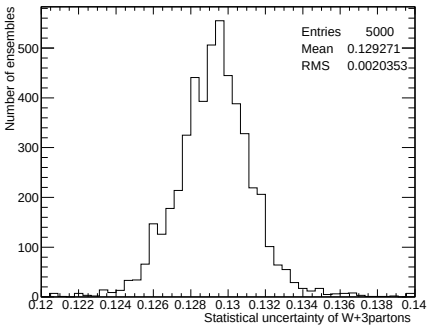

(d) W+3 partons

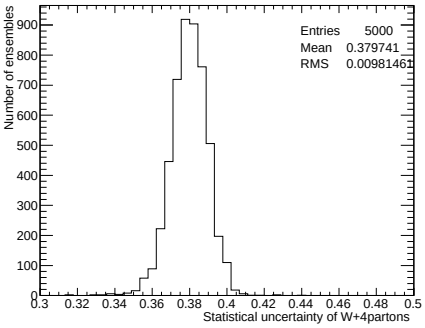

(e) W+4 partons

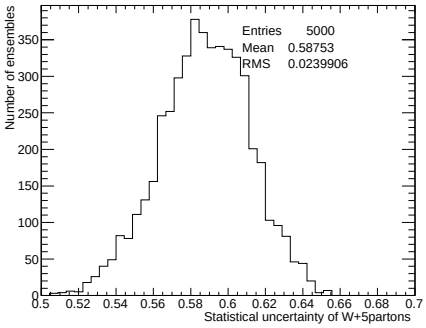

(f) W+5 partons

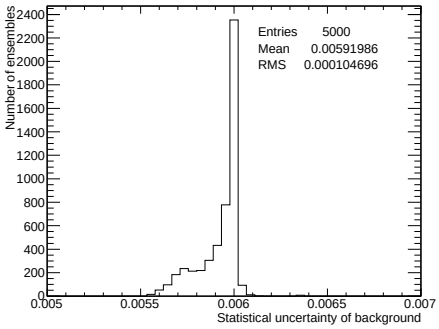

(g) background

Figure 8.7.: Distributions of the statistical uncertainties of the scale factors for the WNp templates and the background.

8.7.2. Systematic Uncertainties

The evaluation of the dominant systematic uncertainties shall be briefly discussed here. One possible approach for the evaluation of systematic uncertainties is via pseudo-data distributions. A pseudo-data set with conditions that are changed within the uncertainties of the systematic source is created. For the uncertainty on the Jet Energy Scale (JES) one obtains for example one distribution for JES scaled up and down, respectively. Ensemble tests are now performed on these distributions as well as on the nominal one (without variation). The means of the parameter distributions for each ensemble are compared to the ones with the nominal ensemble. The difference between them is taken to be the systematic uncertainty. If the differences of up and down variation are not equal, the largest deviation is taken as the systematic uncertainty.
The main sources of systematic uncertainties are discussed below.

Systematic Uncertainties from Signal and Background Modeling

Initial and Final State Radiation

Initial and final state radiation (ISR and FSR) denote radiations of gluons from the partons or from the final state objects. Changing parameters in the modeling of ISR and FSR are expected to have an influence on the jet multiplicity distribution. The uncertainty could be estimated (as is usually done in the ATLAS top group) by creating samples ISR up/down, FSR up/down and ISR up, FSR up as well as ISR down, FSR down and a nominal sample. Then also here ensemble tests should be used and the means of the resulting parameter distributions are compared with the nominal distribution. The largest deviation can then be taken as systematic uncertainty.

Choice of Generator

The shape of the W+jets pseudo-data depends on the MC generator that is used. Systematic uncertainties are evaluated by comparing the predictions of different MC generators. In this case one could compare the ALPGEN W+jets pseudo-data with the ones generated with SHERPA [48].

Systematic Uncertainties from Detector Modeling

Jet Energy Scale

The energy of a jet can be mismeasured due to several effects as e. g. out-of-cone showering, energy leakage or energy loss in dead detector material. Those mismeasurements are summarized in the term "Jet Energy Scale". The JES is expected to have a significant

impact on the systematic uncertainty of the scale factors. Changing the energy of the jets leads to different acceptances due to the jet p_{T} cut. Thus it is expected that the numbers of jets in an event differ and therefore a different jet multiplicity distribution is expected. The mismeasurements of the b-jet energy scale (bJES) is different from the JES for light jets. This is currently taken into account in ATLAS by considering an extra uncertainty of 2.5% on top of the light JES (added in quadrature).

The impact of other systematic sources such as jet energy resolution, jet reconstruction efficiency, b-tagging calibration etc. can be studied. Also here samples with different conditions have to be generated and evaluated using ensemble tests.

9. Conclusion

The results of the analysis are summarized in the following and an outlook to further studies is given.

9.1. Summary

An application for the W+jets background estimation using scale factors for W+jets MC samples from fitting the jet multiplicity distribution of a W+jets enriched sample has been performed on pseudo-data. The tools for this estimate are set up and working. Closure tests such as calibration curves and pull distributions have been performed and show almost no bias. For some pull distributions deviations are observed that are not compatible with the expected values for a unbiased and efficient template fit. Studies towards the reason of this behaviour lead to the assumption that the application of a Gaussian prior on the background template explains the deviant means and sigmas.
Statistical uncertainties have been evaluated. Due to not yet understood effects on the data/MC ratio the fit has not been performed to data. The fit on pseudo-data shows improvements of the data-MC agreement. Due to the limited time of a bachelor's thesis no systematic uncertainties have been evaluated.

9.2. Outlook

Further studies in order to obtain a data-driven W+jets background estimate with the fitting method presented in this thesis have to investigate the observed disagreement of data and MC values. Systematic uncertainties have to be evaluated. A fit in the e+jets channel has to be performed as well. The procedure has to run over the total data set available. Furthermore this method can be cross checked with other data-driven methods for the W+jets background estimation introduced in Section 2.5. Finally, the results of the background estimation can be applied and tested in a W-helicity analysis.

A. Appendix

Process	MC Generator	Cross section [pb]
$t\bar{t}$	MC@NLO	80.201
Single Top (Wt)	MC@NLO	14.581
Single Top ($e\nu$) s-chan.	MC@NLO	0.4685
Single Top ($e\nu$) t-chan.	MC@NLO	7.152
Single Top ($\mu\nu$) s-chan.	MC@NLO	0.4684
Single Top ($\mu\nu$) t-chan.	MC@NLO	7.176
Single Top ($\tau\nu$) s-chan.	MC@NLO	0.4700
Single Top ($\tau\nu$) t-chan.	MC@NLO	7.128
WW	HERWIG	11.75
WZ	HERWIG	3.432
ZZ	HERWIG	0.977

Table A.1.: Used MC samples for the different processes with cross section in the right column ($\sqrt{s} = 7$ TeV).

Process	MC Generator	Cross section [pb]
$W(e\nu)$+Np0	Alpgen/Jimmy	6913.3
$W(e\nu)$+Np1	Alpgen/Jimmy	1293.0
$W(e\nu)$+Np2	Alpgen/Jimmy	377.1
$W(e\nu)$+Np3	Alpgen/Jimmy	100.9
$W(e\nu)$+Np4	Alpgen/Jimmy	25.3
$W(e\nu)$+Np5	Alpgen/Jimmy	6.9
$W(\mu\nu)$+Np0	Alpgen/Jimmy	6935.4
$W(\mu\nu)$+Np1	Alpgen/Jimmy	1281.2
$W(\mu\nu)$+Np2	Alpgen/Jimmy	375.3
$W(\mu\nu)$+Np3	Alpgen/Jimmy	101.1
$W(\mu\nu)$+Np4	Alpgen/Jimmy	25.7
$W(\mu\nu)$+Np5	Alpgen/Jimmy	7.0
$W(\tau\nu)$+Np0	Alpgen/Jimmy	6835.8
$W(\tau\nu)$+Np1	Alpgen/Jimmy	1276.8
$W(\tau\nu)$+Np2	Alpgen/Jimmy	376.6
$W(\tau\nu)$+Np3	Alpgen/Jimmy	100.8
$W(\tau\nu)$+Np4	Alpgen/Jimmy	25.7
$W(\tau\nu)$+Np5	Alpgen/Jimmy	7.0
Wc+Np0	Alpgen	431.3
Wc+Np1	Alpgen	160.1
Wc+Np2	Alpgen	42.5
Wc+Np3	Alpgen	9.9
Wc+Np4	Alpgen	2.3
$Wb\bar{b}$+Np0	Alpgen/Jimmy	45.6
$Wb\bar{b}$+Np1	Alpgen/Jimmy	33.7
$Wb\bar{b}$+Np2	Alpgen/Jimmy	16.7
$Wb\bar{b}$+Np3	Alpgen/Jimmy	6.3
$Wc\bar{c}$+Np0	Alpgen	127.5
$Wc\bar{c}$+Np1	Alpgen	103.2
$Wc\bar{c}$+Np2	Alpgen	51.7
$Wc\bar{c}$+Np3	Alpgen	16.9

Table A.2.: Used MC samples for the different processes with cross section in the right column ($\sqrt{s} = 7$ TeV).

Process	MC Generator	Cross section [pb]
$Z(ee)$+Np0	Alpgen/Jimmy	661.9
$Z(ee)$+Np1	Alpgen/Jimmy	133.3
$Z(ee)$+Np2	Alpgen/Jimmy	40.3
$Z(ee)$+Np3	Alpgen/Jimmy	11.2
$Z(ee)$+Np4	Alpgen/Jimmy	2.7
$Z(ee)$+Np5	Alpgen/Jimmy	0.8
$Z(\mu\mu)$+Np0	Alpgen/Jimmy	657.7
$Z(\mu\mu)$+Np1	Alpgen/Jimmy	132.8
$Z(\mu\mu)$+Np2	Alpgen/Jimmy	39.6
$Z(\mu\mu)$+Np3	Alpgen/Jimmy	11.1
$Z(\mu\mu)$+Np4	Alpgen/Jimmy	2.8
$Z(\mu\mu)$+Np5	Alpgen/Jimmy	0.8
$Z(\tau\tau)$+Np0	Alpgen/Jimmy	657.4
$Z(\tau\tau)$+Np1	Alpgen/Jimmy	133.0
$Z(\tau\tau)$+Np2	Alpgen/Jimmy	40.4
$Z(\tau\tau)$+Np3	Alpgen/Jimmy	11.0
$Z(\tau\tau)$+Np4	Alpgen/Jimmy	2.9
$Z(\tau\tau)$+Np5	Alpgen/Jimmy	0.7
$Z(ee)b\bar{b}$+Np0	Alpgen/Jimmy	6.52
$Z(ee)b\bar{b}$+Np1	Alpgen/Jimmy	2.47
$Z(ee)b\bar{b}$+Np2	Alpgen/Jimmy	0.808
$Z(ee)b\bar{b}$+Np3	Alpgen/Jimmy	0.387
$Z(\mu\mu)b\bar{b}$+Np0	Alpgen/Jimmy	6.52
$Z(\mu\mu)b\bar{b}$+Np1	Alpgen/Jimmy	2.47
$Z(\mu\mu)b\bar{b}$+Np2	Alpgen/Jimmy	0.808
$Z(\mu\mu)b\bar{b}$+Np3	Alpgen/Jimmy	0.387
$Z(\tau\tau)b\bar{b}$+Np0	Alpgen/Jimmy	6.52
$Z(\tau\tau)b\bar{b}$+Np1	Alpgen/Jimmy	2.47
$Z(\tau\tau)b\bar{b}$+Np2	Alpgen/Jimmy	0.808
$Z(\tau\tau)b\bar{b}$+Np3	Alpgen/Jimmy	0.387

Table A.3.: Used MC samples for the different processes with cross section in the right column ($\sqrt{s} = 7$ TeV).

B. Appendix

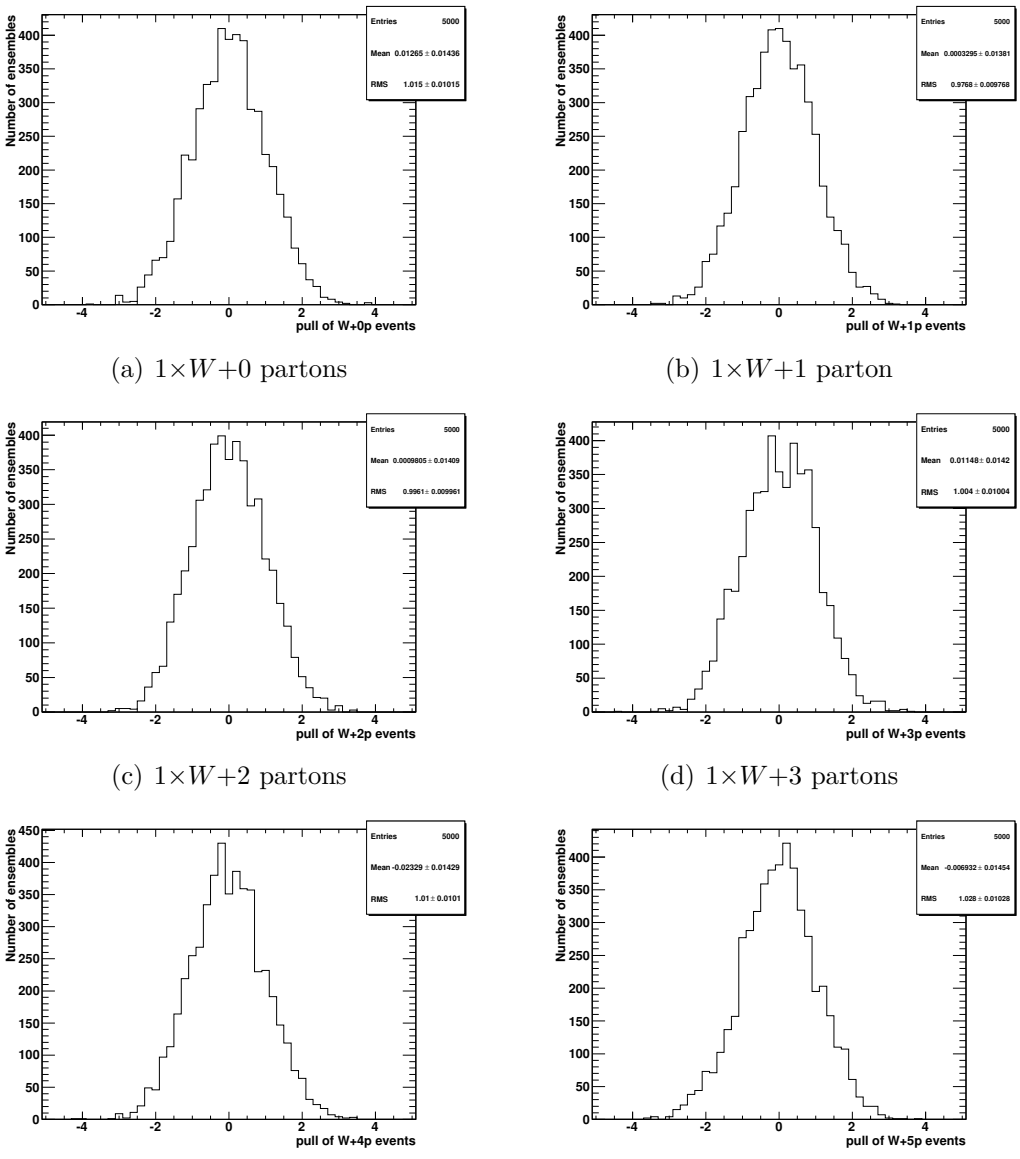

(a) 1×W+0 partons

(b) 1×W+1 parton

(c) 1×W+2 partons

(d) 1×W+3 partons

(e) 1×W+4 partons

(f) 1×W+5 partons

Figure B.1.: Pull distribution for the W+N partons templates, each unscaled (scale factor =1).

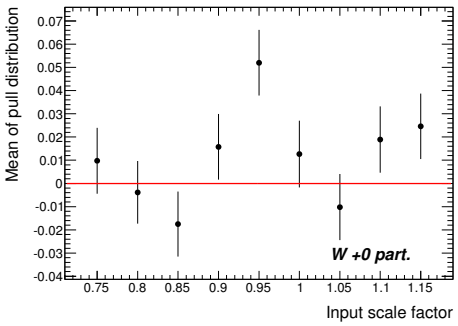

(a) W+0 partons

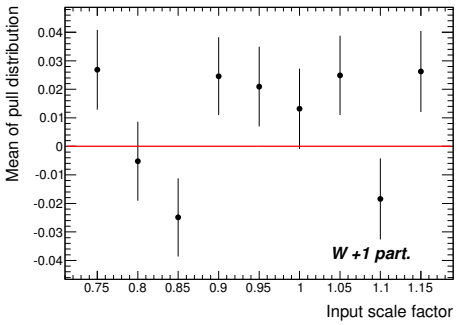

(b) W+1 parton

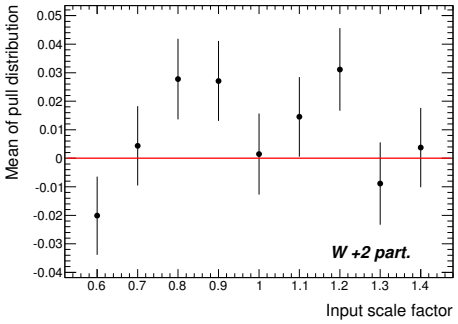

(c) W+2 partons

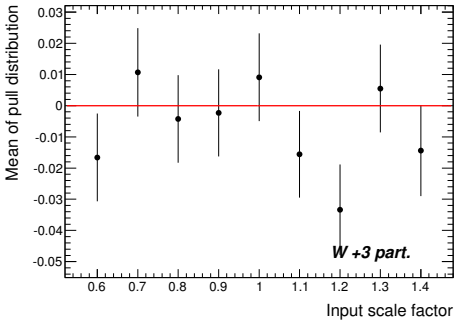

(d) W+3 partons

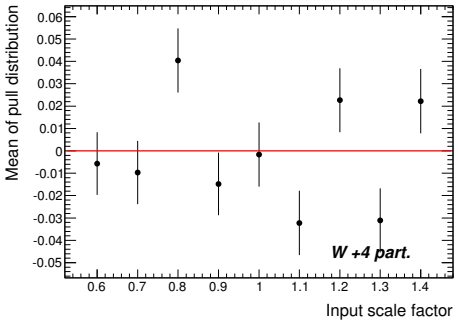

(e) W+4 partons

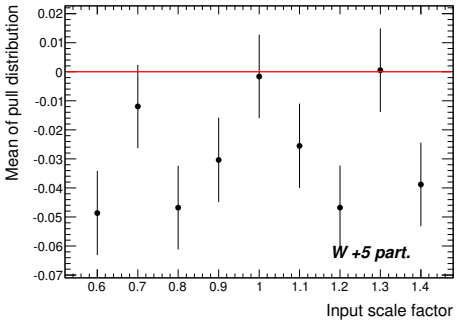

(f) W+5 partons

Figure B.2.: Plots of the means of the pull distributions as a function of the input scale factors for the WNp samples.

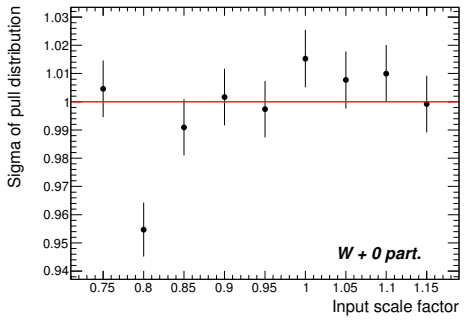

(a) W+0 partons

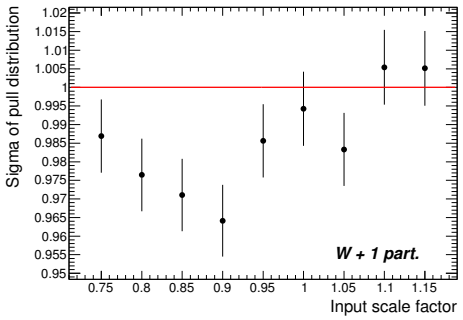

(b) W+1 parton

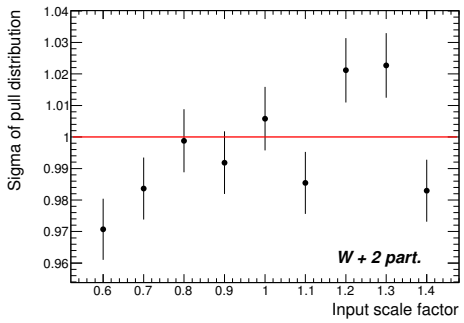

(c) W+2 partons

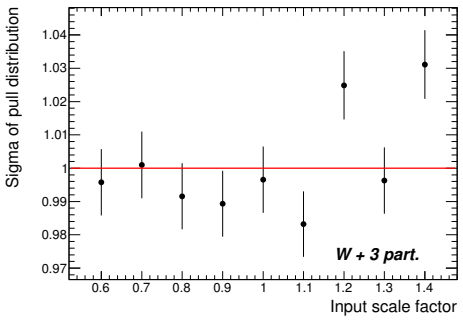

(d) W+3 partons

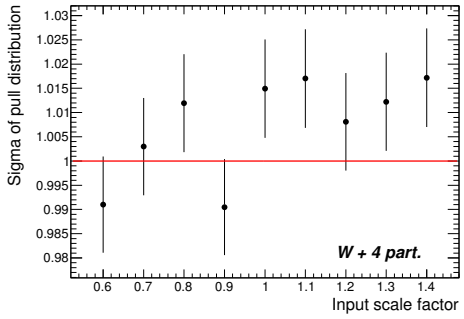

(e) W+4 partons

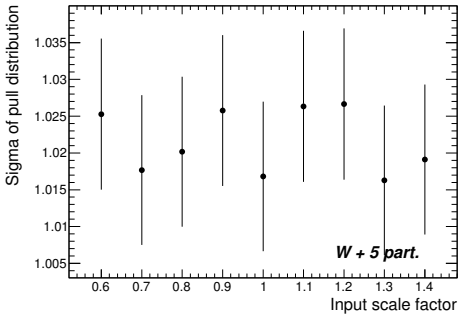

(f) W+5 partons

Figure B.3.: Plots of the sigmas of the pull distributions as a function of the input scale factors for the WNp samples.

C. Appendix

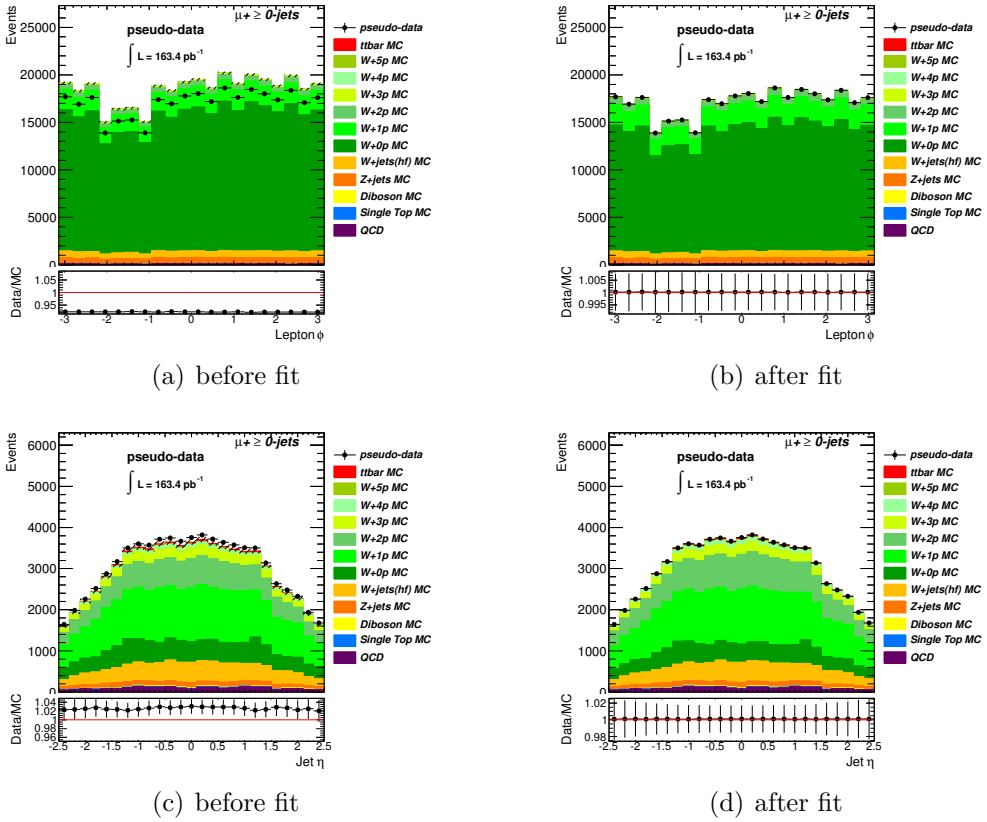

(a) before fit

(b) after fit

(c) before fit

(d) after fit

Figure C.1.: Comparison of distributions before and after applying the fitted scale factors.

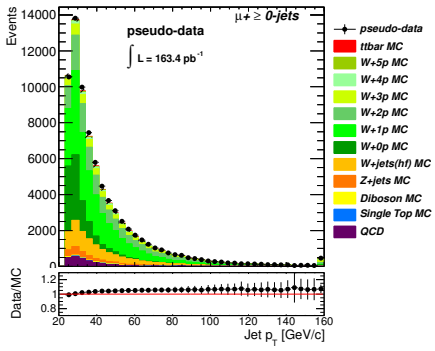

(a) before fit

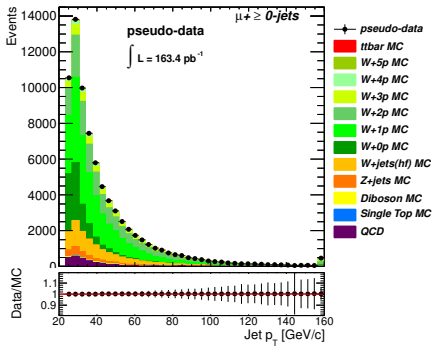

(b) after fit

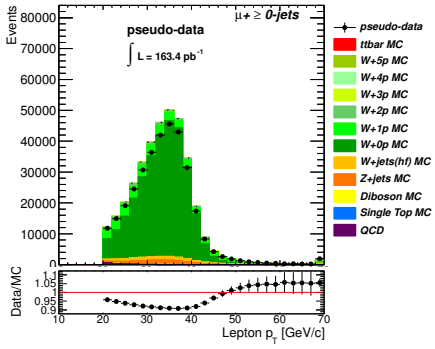

(c) before fit

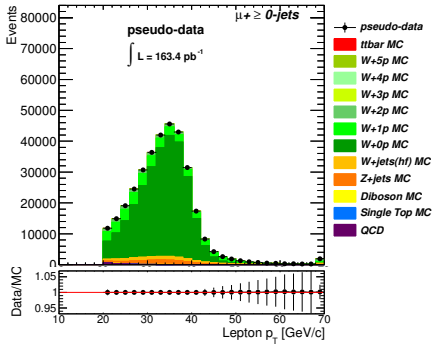

(d) after fit

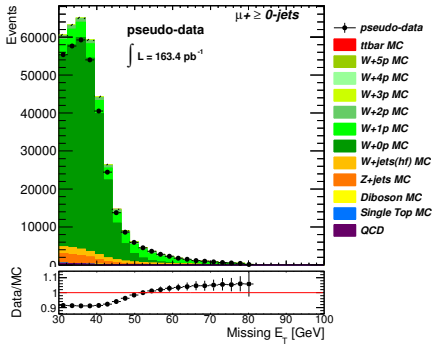

(e) before fit

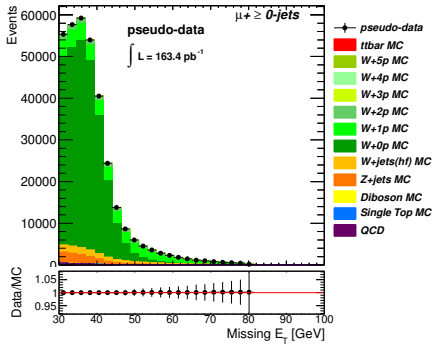

(f) after fit

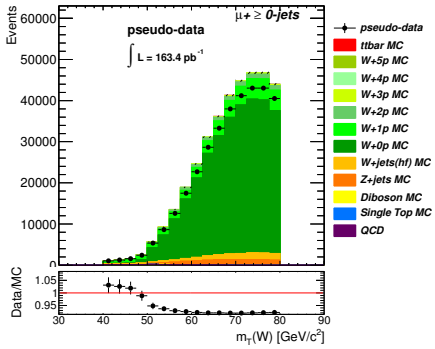

(g) before fit

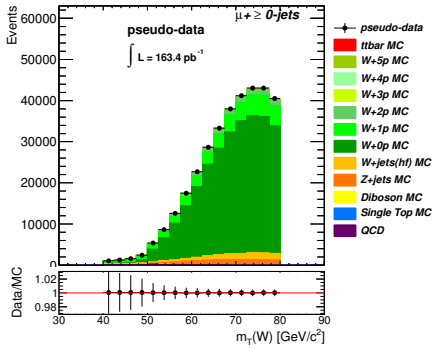

(h) after fit

Figure C.2.: Comparison of distributions before and after applying the fitted scale factors.

Bibliography

[1] Tevatron Electroweak Working group (CDF and DØ), *Combination of CDF and DØ Results on the Mass of the Top Quark* (2010), 1007.3178

[2] K. Nakamura et al. (Particle Data Group), J.Phys. **G37(075021)** (2010)

[3] S. Weinberg, *A Model of Leptons*, Phys. Rev. Lett. **19**, 1264 (1967)

[4] A. Salam, *Weak and Electromagnetic Interactions*, ed. Nobel Symposium No. 8 (Almqvist & Wiksell, Stockholm, 1968)

[5] H. Georgi, S. L. Glashow, *Unified Weak and Electromagnetic Interactions without Neutral Currents*, Phys. Rev. Lett. **28**, 1494 (1972)

[6] D. Griffiths, *Introduction to Elementary Particles*, 2nd, revised Edition, WILEY-VCH, Weinheim (2008)

[7] B. Kayser, *Neutrino Mass, Mixing, and Flavor Change* (2008), 0804.1497

[8] S. Abachi, et al. (DØ), *Observation of the Top Quark*, Phys. Rev. Lett. **74**, 2632 (1995), hep-ex/9503003

[9] F. Abe, et al. (CDF), *Observation of Top Quark Production in $p\bar{p}$ Collisions with the Collider Detector at Fermilab*, Phys. Rev. Lett. **74**, 2626 (1995), hep-ex/9503002

[10] I. I. Y. Bigi et al., Phys. Lett. **B181**, 157 (1986)

[11] T. M. Liss, A. Quadt (Particle Data Group), *The Top Quark*, Phys. Review (2010)

[12] C. Berger, *Elementarteilchenphysik*, 2. Aufl., Springer (2006)

[13] V. M. Abazov, et al. (DØ), *Measurement of the W boson helicity in top quark decays using 5.4 fb^{-1} of $p\bar{p}$ collision data*, Phys. Rev. **D83**, 032009 (2011), 1011.6549

[14] M. Cacciari et al., Sov. Phys. **JETP 04**, 068 (2004)

[15] S. Pashapour, *First Measurement of* $\sigma(gg \to t\bar{t})/\sigma(p\bar{p} \to t\bar{t})$, Ph.D. Thesis, University of Toronto (2008)

[16] H.-L. Lai, et al., *New parton distributions for collider physics*, Phys. Rev. **D82**, 074024 (2010), 1007.2241

[17] CMS Collaboration, *Rates of Jets Produced in Association with W and Z Bosons* (2011)

[18] C. F. Berger et al., *Precise Predictions for W + 4-Jet Production at the Large Hadron Collider*, Physical Review Letters **106** (2011)

[19] *Measurement of the W-boson polarisation in top quark decays in pp collision data at* $\sqrt{s}$ *= 7 TeV using the ATLAS detector*, Technical Report ATLAS-CONF-2011-037, CERN, Geneva (2011)

[20] *Measurement of the top quark-pair cross-section with ATLAS in pp collisions at sqrt(s) = 7 TeV in the single-lepton channel using b-tagging*, Technical Report ATLAS-CONF-2011-035, CERN, Geneva (2011)

[21] F. A. Berends, H. Kuijf, B. Tausk, W. T. Giele, *On the production of a W and jets at hadron colliders*, Nuclear Physics B **357(1)**, 32 (1991)

[22] S. Ellis, R. Kleiss, W. Stirling, *W's, Z's and jets*, Physics Letters B **154(5-6)**, 435 (1985)

[23] M. Barisonzi et al., *A Search for* $t\bar{t}$ *Resonances in the Lepton Plus Jets Channel in 35* pb^{-1} *of pp Collisions at* $\sqrt{s} = 7$ *TeV*, Technical Report ATL-COM-PHYS-2011-070, CERN, Geneva (2011)

[24] Luminosity Public Results - Luminosity 2011 *pp* collisions ATLAS Public Results (2011), URL https://twiki.cern.ch/twiki/bin/view/AtlasPublic/LuminosityPublicResults#2011_pp_Collisions

[25] G. Aad, E. Abat, J. Abdallah, A. Abdelalim, A. Abdesselam, O. Abdinov, B. Abi, M. Abolins, H. Abramowicz, E. Acerbi, et al., *The ATLAS experiment at the CERN large hadron collider*, Journal of Instrumentation **3**, S08003 (2008)

[26] E. O. for Nuclear Research (Ginebra), *ATLAS detector and physics performance: Technical Design Report*, CERN (1999)

[27] M. A. Dobbs, et al., *Les Houches guidebook to Monte Carlo generators for hadron collider physics* (2004), hep-ph/0403045

[28] S. Agostinelli et al., *GEANT4–A simulation toolkit*, Nucl. Instrum. Meth. **506(3)**, 250 (2003)

[29] M. L. Mangano, M. Moretti, F. Piccinini, R. Pittau, A. D. Polosa, *ALPGEN, a generator for hard multiparton processes in hadronic collisions*, JHEP **0307**, 001 (2003)

[30] G. Corcella, et al., *HERWIG 6.5: an event generator for Hadron Emission Reactions With Interfering Gluons (including supersymmetric processes)*, JHEP **01**, 010 (2001), hep-ph/0011363

[31] J. M. Butterworth, J. R. Forshaw, M. H. Seymour, *Multiparton interactions in photoproduction at HERA*, Z. Phys. **C72**, 637 (1996), hep-ph/9601371

[32] M. L. Mangano, *Merging multijet matrix elements and shower evolution in hadronic collisions*, Talk, Lund University (2004), URL http://cern.ch/mlm/talks/lund-alpgen.pdf

[33] S. Frixione, P. Nason, B. R. Webber, *Matching NLO QCD and parton showers in heavy flavour production*, JHEP **08**, 007 (2003), hep-ph/0305252

[34] G. Aad, et al. (Atlas), *Measurement of the $W\to \ell\nu$ and $Z/\gamma^* \to \ell\ell$ production cross sections in proton-proton collisions at sqrt(s) = 7 TeV with the ATLAS detector*, JHEP **12**, 060 (2010), 1010.2130

[35] K. Bachas, *A measurement of the ATLAS muon reconstruction and trigger efficiency using J/psi decays*, Technical Report ATLAS-COM-CONF-2011-002, CERN, Geneva (2011),

[36] M. Cacciari, G. P. Salam, G. Soyez, *The anti-k_t jet clustering algorithm* (2008), URL doi:10.1088/1126-6708/2008/04/063

[37] B. Alvarez et al., *b-jet Tagging for Top Physics: Perfomance studies, Calibrations and Heavy Flavor Fractions*, Technical Report ATL-COM-PHYS-2011-124, CERN, Geneva (2011)

[38] N. Benekos, *Lepton trigger and identification for the Winter 2011 top quark analyses*, Technical Report ATL-COM-PHYS-2011-123, CERN, Geneva (2011), supporting document for Winter 2011 top physics measurements

[39] The ATLAS Collaboration, *Muon Momentum Resolution in First Pass Reconstruction of pp Collision Data Recorded by ATLAS in 2010* (2011)

[40] G. D'Agostini, *Bayesian Reasoning in Data Analysis - A Critical Introduction*, World Scientific (2003)

[41] D. Kollár, K. Kröninger, A. Caldwell *BAT - The Bayesian Analysis Toolkit*, Computer Physics Communications **180** (2009)

[42] C. Robert, G. Casella, *Monte Carlo statistical methods*, Springer Verlag (2004)

[43] F. James, *MINUIT—A System for Function Minimization and Analysis of the Parameter Errors and Correlations*, Computer Physics Communications **10**, 343 (1975)

[44] K. Kröninger, *Estimating contributions from different processes - A Bayesian approach to the template method*, ATL-COM-PHYS-2010-186 (2010)

[45] M. L. Mangano, *Private Communications* (2011)

[46] S.Allwood-Spires et al., *Monte Carlo samples used for top physics* ATL-PHYS-INT-2010-132 (2010), URL `http://cdsweb.cern.ch/record/1312945/files/ATL-PHYS-INT-2010-132.pdf`

[47] G. Aad, et al. (Atlas), *Measurement of the top quark-pair production cross section with ATLAS in pp collisions at* $\sqrt{s} = 7\ TeV$ (2010), `1012.1792`

[48] T. Gleisberg, S. Höche, F. Krauss, A. Schälicke, S. Schumann, J. Winter, *SHERPA 1. α, a proof-of-concept version*, Journal of High Energy Physics **2004**, 056 (2004)

Acknowledgement

I am very grateful to Andrea Knue, who supervised me in the last eighteen weeks. Despite the physical distance she was always available and ready to help. Her patience, endless effort and understanding helped me to survive especially the last days. Thank you very much!
I also would like to thank Shabnaz Pashapour for a lot of helpful discussions and also supervising me. In this context I also have to thank Kevin Kroeninger for his readiness and talent to explain issues in a manner so that everyone understands.
Additional thanks go to my first referee Prof. Dr. Arnulf Quadt for giving me the oppurtunity to write my bachelor's thesis in the HEP and letting me have a look into the world of research. I would also like to express my gratitude for giving me the oppurtunity to participate in the summer students programme at DESY. I also would like to thank Prof. Dr. Ariane Frey for her readiness to be the second referee.
Furthermore I would like to thank my family and friends for their continious support.

Erklärung nach §13(8) der Prüfungsordnung für den Bachelor-Studiengang Physik und den Master-Studiengang Physik an der Universität Göttingen:

Hiermit erkläre ich, dass ich diese Abschlussarbeit selbständig verfasst habe, keine anderen als die angegebenen Quellen und Hilfsmittel benutzt habe und alle Stellen, die wörtlich oder sinngemäß aus veröffentlichten Schriften entnommen wurden, als solche kenntlich gemacht habe.
Darüberhinaus erkläre ich, dass diese Abschlussarbeit nicht, auch nicht auszugsweise, im Rahmen einer nichtbestandenen Prüfung an dieser oder einer anderen Hochschule eingereicht wurde.

Göttingen, den 25. Oktober 2011

(Cora Fischer)